

Research Article

Title: Ependymal cell lineage reprogramming as a potential therapeutic intervention for hydrocephalus

Authors: Konstantina Kaplani¹, Maria - Eleni Lalioti¹, Stella Vassalou¹, Georgia Lokka¹, Evangelia Parlapani¹, Georgios Kritikos¹, Zoi Lygerou², Stavros Taraviras¹,

Affiliations:

¹Department of Physiology, School of Medicine, University of Patras, Patras, Greece

²Department of General Biology, School of Medicine, University of Patras, Patras, Greece

Corresponding author: Stavros Taraviras

Corresponding author's address: Department of Physiology, School of Medicine, University of Patras, Asklepiou Street 1, Rio 26504, Patras, Greece

Corresponding author's phone and fax: +30 2610 997676

Corresponding author's e-mail address: taraviras@med.upatras.gr

Reaction with $\text{Cu}(\text{ClO}_4)_2 \cdot \text{MeOH}$ gave a complex mixture.

$$K = \begin{pmatrix} 1 & -1 & 1 & 1 & 1 \\ -1 & 1 & -1 & 1 & 1 \\ 1 & -1 & 1 & -1 & 1 \\ 1 & 1 & -1 & -1 & 1 \\ 1 & 1 & 1 & 1 & -1 \end{pmatrix}, M = \begin{pmatrix} 1 & 1 & 1 & 1 & 1 \\ 1 & 1 & 1 & 1 & 1 \\ 1 & 1 & 1 & 1 & 1 \\ 1 & 1 & 1 & 1 & 1 \\ 1 & 1 & 1 & 1 & 1 \end{pmatrix}, L = \begin{pmatrix} 1 & 1 & 1 & 1 & 1 \\ 1 & 1 & 1 & 1 & 1 \\ 1 & 1 & 1 & 1 & 1 \\ 1 & 1 & 1 & 1 & 1 \\ 1 & 1 & 1 & 1 & 1 \end{pmatrix}$$

Keywords: ependymal cells, reprogramming, hydrocephalus, McIdas, GemC1

23 **ABSTRACT**

24 Hydrocephalus is a common neurological condition, characterized by the excessive accumulation of
25 cerebrospinal fluid in the cerebral ventricles. Primary treatments for hydrocephalus mainly involve
26 neurosurgical cerebrospinal fluid diversion, which hold high morbidity and failure rates, highlighting the
27 necessity for the discovery of novel therapeutic approaches. Although the pathophysiology of
28 hydrocephalus is highly multifactorial, impaired function of the brain ependymal cells plays a
29 fundamental role in hydrocephalus. Here we show that GemC1 and McIdas, key regulators of
30 multiciliated ependymal cell fate determination, induce direct cellular reprogramming towards
31 ependyma. Our study reveals that ectopic expression of GemC1 and McIdas reprograms cortical
32 astrocytes and programs mouse embryonic stem cells into ependyma. McIdas is sufficient to establish
33 functional activity in the reprogrammed astrocytes. Furthermore, we show that McIdas' expression
34 promotes ependymal cells regeneration in two different postnatal hydrocephalus mouse models: an
35 intracranial hemorrhage and a genetic form of hydrocephalus and ameliorates the cytoarchitecture of the
36 neurogenic niche. Our study provides evidence on the restoration of ependyma in animal models
37 mimicking hydrocephalus that could be exploited towards future therapeutic interventions.

38

39

40

41

42

43

44

45

46

47 **INTRODUCTION**

48 Hydrocephalus is a neurological disorder defined by the abnormal accumulation of cerebrospinal fluid
49 (CSF) within the brain ventricles, leading to increased head circumference (Schrandt-Stumpel & Fryns,
50 1998). The condition can arise as a primary clinical feature triggered by a genetic cause (congenital
51 hydrocephalus) or secondary (acquired hydrocephalus) to other insults such as central nervous system
52 (CNS) infections, tumors, trauma, or hemorrhage (Rekate, 2009; Kahle *et al*, 2016; Kousi & Katsanis,
53 2016). Malfunction of the ependymal cells is a leading cause of the pathophysiological mechanism of
54 hydrocephalus as these cells have a key role in CSF circulation and composition (Ji *et al*, 2022). In
55 addition, hydrocephalus is linked with disorganization of the subventricular neurogenic niche's
56 cytoarchitecture and neurogenesis defects, as ependymal cells were shown to provide structural and
57 functional support to the adult neural stem cells (Paez-Gonzalez *et al*, 2011; McAllister, James P. *et al*,
58 2017; Rodríguez & Guerra, 2017).

59 Under homeostatic conditions, ependymal cells form one of the largest epithelia of the brain, lying
60 adjacent to the ventricular lumen and bear unique structural characteristics. The cell surface exposed to
61 the ventricular lumen contains a patch of approximately 50 modified centrioles, called basal bodies,
62 which are tiny microtubule-based organelles responsible for nucleating an equal number of motile cilia.
63 Cilia are anchored on their apical surface, beating in the same direction and in a coordinated fashion,
64 thus contributing to efficient CSF circulation throughout the brain (Mirzadeh *et al*, 2008, 2010).
65 Constant ciliary beating facilitates secreted molecules dispersion to other regions of the CNS. Such
66 circulating molecules in the CSF influence neurogenesis and neuroblasts' migration to the olfactory
67 bulbs (Lim *et al*, 2000; Sawamoto *et al*, 2006).

68 Ependymal cell differentiation is a multi-step process orchestrated by a tightly regulated transcriptional
69 program which is responsible for activating numerous genes that promote amplification and docking of
70 centrioles and the formation of cilia (Kyrousi *et al*, 2017; Arbi *et al*, 2018). We have previously
71 provided evidence that the Geminin family proteins, GEMC1 and MCIDAS, are the earliest regulators
72 for the cell fate commitment to the ependymal lineage (Kyrousi *et al*, 2015). *GemC1* lies upstream of
73 *Mcidas* inducing its transcriptional activation, while both upregulate genes that are essential for centriole
74 amplification and for promoting the downstream transcriptional machinery of multiciliogenesis (Kyrousi
75 *et al*, 2015; Arbi *et al*, 2016; Lalioti *et al*, 2019a). GEMC1 and MCIDAS cooperate with E2F4/5

76 transcription factors, to upregulate *cMyb* and *Ccno*, which are implicated in centriole amplification (Tan
77 *et al*, 2013; Wallmeier *et al*, 2014; Funk *et al*, 2015; Arbi *et al*, 2018). In addition, we and others have
78 provided evidence that *GemC1* and *McIdas* drive the transcriptional activation of P73 and FOXJ1
79 transcription factors, which are implicated in basal bodies docking and cilia motility (Kyrousi *et al*,
80 2015; Arbi *et al*, 2016; Nemajerova *et al*, 2016; Marshall *et al*, 2016; Lalioti *et al*, 2019a).

81 Given the multifaceted roles that ependymal cells have in hydrocephalus pathophysiology, restoration of
82 ependymal cells could significantly contribute to hydrocephalus therapy. With the advancements in
83 direct reprogramming-based strategies for conditions affecting the central nervous system (Bocchi *et al*,
84 2022), it is plausible to anticipate that cellular reprogramming directed towards ependymal cells could
85 represent a significant breakthrough in the treatment of hydrocephalus. In the present study we showed
86 that ectopic expression of *GemC1* or *McIdas* promotes programming of mouse pluripotent embryonic
87 stem cells and reprogramming of cortical astrocytes into ependymal cells, with *McIdas* being more
88 efficient on establishing functional motile cilia in reprogrammed astrocytes. In addition, forced
89 expression of *McIdas* in both a genetic and an acquired hydrocephalus mouse model promoted *in vivo*
90 reprogramming of cells residing in the ventricular walls of the diseased brain into functional ependymal
91 cells. Importantly, reprogrammed ependymal cells were able to beat their cilia in a coordinated fashion
92 and formed pinwheel structures together with neural stem cells in hydrocephalic mice, revealing their
93 potential to regenerate the architecture of the neurogenic niche, which is disrupted in hydrocephalus.
94 Collectively, our data suggest that GEMC1 and MCIDAS can orchestrate the transcriptional program of
95 multiciliogenesis establishing ependymal cell fate and differentiation, providing proof of principle
96 evidence that restoration of ependymal cells could potentially contribute to hydrocephalus management.

97

98

99

100 **RESULTS**

101 **GemC1 and McIdas promote programming of mouse embryonic stem cells and reprogramming of
102 cortical astrocytes into ependymal cells**

103 *GemC1* and *McIdas* are the most upstream regulators driving multiciliogenesis in vertebrate organisms
104 (Stubbs *et al*, 2012; Ma *et al*, 2014; Boon *et al*, 2014; Kyrousi *et al*, 2015; Terré *et al*, 2016; Arbi *et al*,
105 2016). We therefore postulated that *GemC1* and *McIdas* would be capable of inducing stem cell
106 programming towards multiciliated ependymal cells. To examine this hypothesis, mouse embryonic
107 stem cells (mESCs) were transfected with plasmids encoding *McIdas* or *GemC1* in conjunction with
108 GFP (referred to as McIdas and GemC1 respectively), or GFP alone as a control. Transfected mESCs
109 were cultured for four days in the absence of Leukemia Inhibitory Factor (LIF) and subjected to
110 immunostaining for FoxJ1, a key transcription factor for the differentiation of ependymal cells, and
111 Pericentrin which marks nascent basal bodies (Fig EV1A). Our analysis showed that 87% of *McIdas*-
112 and 39% of *GemC1*-overexpressing mESCs were expressing FoxJ1, while only 1% FoxJ1 positive cells
113 were detected in the control (Fig EV1B). In addition, we identified that 90% of McIdas- and 59% of
114 GemC1-overexpressing mESCs showed accumulation of Pericentrin staining (Fig EV1C), thus
115 presented multiple nascent basal bodies, corresponding to differentiating ependymal cells. Furthermore,
116 we examined whether McIdas and GemC1-overexpressing mESCs acquire multiple cilia, a unique
117 structural characteristic of the ependymal cells. Double immunofluorescence experiments were
118 performed six days following mESCs transfection using anti-Pericentrin and anti-acetylated-a-tubulin
119 antibodies to mark the basal bodies and cilia, respectively (Fig EV1D). Our analysis revealed that 66%
120 of McIdas- and 21% of GemC1- overexpressing mESCs develop multiple cilia arising from numerous
121 basal bodies. On the contrary, control mESCs develop neither multiple basal bodies nor cilia (Fig

122 EV1D, E). Our data show that ectopic expression of *McIdas* and *GemC1* programs mESCs into
123 multiciliated ependymal cells.

124 Next, we sought out to explore the reprogramming potential of *McIdas* and *GemC1* in astrocytes that
125 under physiological conditions do not differentiate into ependymal cells. Astrocytes were isolated from
126 the cortex of neonatal mice and were subsequently infected with lentiviruses expressing GFP-McIdas or
127 GFP-GemC1 (referred to as McIdas and GemC1, respectively), while lentiviruses expressing GFP alone
128 were used as control. Cells were subsequently cultured under differentiating conditions and
129 immunofluorescence experiments were conducted to assess the expression of known ependymal and
130 astrocytic markers (Fig. 1A). Ectopic expression of both *McIdas* and *GemC1* resulted in *P73* expression,
131 a marker of the early steps of ependymogenesis, in 37% and 36% of McIdas- and GemC1- infected
132 cells, respectively, while in the control condition only 4% of the transduced cells was expressing *P73*
133 (Fig. 1B, C, and EV 2A, B). Notably, concurrent changes in the expression pattern of the astrocytic
134 marker *S100 β* were observed in approximately 20% of McIdas- and 18% of GemC1- infected
135 astrocytes, as *S100 β* expression was detected around their cell body, which is characteristic for
136 ependymal cells (Mirzadeh *et al*, 2008) (Fig. 1B-D and EV. 2A-C). On the contrary, control astrocytes
137 retained a cytoplasmic expression of the *S100 β* protein, a typical feature of astrocytes. Overall, our data
138 suggest that ectopic expression of McIdas and GemC1 can lead to the acquisition of the ependymal cell
139 fate.

140 Subsequently, we examined whether McIdas- and GemC1-transduced astrocytes successfully
141 differentiate into ependymal cells. We performed immunofluorescence experiments using specific
142 antibodies recognizing FoxJ1 and Pericentrin, to identify astrocytes that acquired the ependymal fate and
143 successfully managed to multiply their basal bodies, respectively. Our analysis showed that fourteen

144 days post infection 49% of McIdas- and 19% of GemC1- infected astrocytes were expressing FoxJ1
145 (Fig. 1E, F and EV2D, E). In addition, 28% of the McIdas- and 12% of GemC1- infected astrocytes
146 possessed multiple basal bodies, indicated by the accumulation of Pericentrin signal (Fig. 1G and
147 EV2F). Moreover, expression of a GFP lentivirus did not result into FoxJ1 expression nor accumulation
148 of Pericentrin.

149 In addition, we examined the ability of McIdas and GemC1 to repress the astrocytic identity of the
150 transduced astrocytes. Towards this direction, the combined expression of the astrocytic markers GFAP
151 and S100 β was assessed through immunofluorescence experiments at fourteen days post infection. Our
152 analysis revealed that McIdas ectopic expression resulted to 23% of GFAP+/S100 β + double positive
153 cells compared to 31% in the control condition (Appendix Fig. S1A, B). We did not observe statistically
154 significant change in the percentage of GFAP+/S100 β + double positive cells following GemC1 ectopic
155 expression (Appendix Fig. S1C). In addition, we examined the percentage of infected cells that were
156 GFAP- and reveal S100 β expression around the cell body, which correspond to ependymal cells. We
157 showed that 28% McIdas- and 22% GemC1- infected astrocytes present this expression pattern
158 (Appendix Fig. S1A, B), which is in accordance with our analysis performed in earlier stages of
159 reprogramming (Fig. 1D). Our results indicate that a significant percentage of the infected astrocytes are
160 reprogrammed to the ependymal lineage and possess unique ependymal morphological characteristics.
161 Moreover, we showed that McIdas is more potent in the downregulation of the astrocytic identity of the
162 transduced cells.

163 GemC1 is positioned upstream of McIdas in the molecular pathway governing ependymogenesis, as it
164 regulates the transcriptional activation of McIdas and controls the initial fate commitment towards the
165 ependymal lineage (Kyrousi *et al*, 2015, 2017). Our results suggest that GemC1 was less effective than

166 McIdas in reprogramming of astrocytes. We have therefore examined whether ectopic expression of
167 GemC1 in astrocytes would not induce McIdas expression at sufficient levels. To test this hypothesis,
168 we conducted immunofluorescence experiments using an McIdas specific antibody and quantified
169 McIdas fluorescence in McIdas- and GemC1-infected astrocytes seven days post infection (Appendix
170 Fig. S2A). Our results revealed that McIdas' ectopic expression led to higher expression levels
171 compared to GemC1 (Appendix Fig. S2B), providing a potential mechanism for their differential ability
172 to induce reprogramming.

173 Given the greater capacity of *McIdas* to induce the ependymal differentiation in astrocytes compared to
174 *GemC1*, we hypothesized that *McIdas* would reprogram cortical astrocytes into fully mature ependymal
175 cells carrying multiple basal bodies nucleating motile cilia. To address this point, we initially performed
176 immunofluorescence experiments in transduced astrocytes twenty-two days post infection using
177 antibodies against Centriolin (also known as Cep110), a known centrosomal marker, and Meig1 which
178 was recently characterized as ependymal cell marker (MacDonald *et al*, 2021). We detected
179 accumulation of both Centriolin (Appendix Fig.S3A) and Meig1 (Appendix Fig.S3B) signal in McIdas-
180 infected astrocytes, verifying the generation of multiple basal bodies upon McIdas' ectopic expression.
181 Next, we performed immunofluorescence experiments making use of antibodies against acetylated a-
182 tubulin, which stains ciliary axonemes, and the astrocytic marker glial fibrillary acidic protein (GFAP).
183 The ectopic expression of *McIdas* resulted in the downregulation of GFAP expression and the
184 generation of multiple cilia on the surface of the reprogrammed astrocytes, revealing the loss of the
185 astrocytic identity and the establishment of the ependymal differentiation (Fig. 2A). Our analysis
186 showed that 18% of McIdas- infected astrocytes were reprogrammed into multiciliated ependymal cells
187 based on acetylated-a-tubulin staining (Fig. 2C), which was consistent with the percentage of McIdas-
188 infected cells that downregulate the expression of the astrocytic marker GFAP (Fig. 2B). Additionally,

189 live imaging microscopy experiments were performed in transduced astrocytes twenty-two days post
190 infection to address the ability of the reprogrammed astrocytes multicilia to beat (Movies EV1-4). Using
191 high-speed video microscopy, we acquired fast video recordings from GFP (Movies EV1-2) and
192 McIdas- infected astrocytes (Movies EV3-4), which revealed the presence of ciliary motility in McIdas-
193 infected cells as opposed to the absence of motility in GFP- infected cells. Importantly, our analysis
194 showed that McIdas expression established cilia movement that was sufficient to propel fluorescent
195 particles added to the imaging medium, highlighting the functionality of the ependymal cells and their
196 capability to create a fluid flow. On the contrary, astrocytes infected with a control virus were unable to
197 propel the fluorescent particles, as were only observed to have a rather stable forward and backward
198 motion (Fig. 2D).

199 Our findings show that GemC1 and McIdas promote the early steps of the multiciliogenesis program in
200 both embryonic stem cells and astrocytes. Importantly, McIdas has a greater capacity for eliciting direct
201 reprogramming into functional ependymal cells.

202

203 **McIdas induces ependymal cells regeneration in a mouse model of intracranial hemorrhage**
204 **hydrocephalus**

205 In both human and murine hydrocephalus, the disrupted ependymal cell population is replaced by
206 astrocytes. However, this astrocitic scarring along the denuded ventricular wall fails to restore the
207 ependymal functions (Sival *et al*, 2011; Roales-Buján *et al*, 2012; Guerra *et al*, 2015; McAllister, James
208 P. *et al*, 2017). Based on our finding that *McIdas* can successfully reprogram cortical astrocytes into
209 functional ependymal cells, we examined whether *McIdas* could induce direct reprogramming of
210 periventricular cells in hydrocephalic models. We used an established mouse model of intracranial

211 hemorrhage hydrocephalus induced by the elevated concentration of Lysophosphatidic Acid (LPA) in
212 the brain (Yung *et al*, 2015; Lummis *et al*, 2019), which closely mirrors the most common type of
213 human hydrocephalus.

214 Based on previously established protocols (Yung *et al*, 2011; Lummis *et al*, 2019), postnatal day five
215 (P5) mice received intracranial injections of LPA and mouse brains were examined two days later to
216 evaluate hydrocephalus occurrence. Although no obvious differences were observed in the size of LPA-
217 treated brains macroscopically (Fig. EV3A), coronal brain sections revealed ventricular dilation in LPA-
218 injected animals compared to non-injected ones (Fig. EV3B), confirming the development of
219 hydrocephalus. In addition, acetylated-a-tubulin immunofluorescence revealed the ciliary disruption in
220 ependymal cells alongside the ventricular walls upon LPA administration (Fig. EV3C), in line with
221 previous studies (Lummis *et al*, 2019). On the contrary, ependymal cells with multiple cilia covered the
222 entire ventricular walls in control animals (Fig. EV3C). Given that the ventricular walls of the LPA-
223 injected hydrocephalic mice were denuded from ependymal cells we wished to determine their cellular
224 composition. We performed immunofluorescence with an antibody against the astrocytic marker glial
225 fibrillary acidic protein (GFAP). Our analysis showed that GFAP positive cells with long processes,
226 which likely corresponded to reactive astrocytes, covered the walls of the lateral ventricles in regions
227 where ependymal cells localize under physiological conditions (Fig. EV3C), in line with previous
228 findings (Roales-Buján *et al*, 2012).

229 To assess whether McIdas can induce direct reprogramming into ependyma in LPA-induced
230 hydrocephalus, GFP-McIdas (McIdas) or GFP expressing plasmids were electroporated onto P7 brains
231 isolated from LPA-treated mice by targeting the dorsolateral wall of one lateral ventricle to introduce
232 plasmids in cells located at periventricular regions. Subsequently, thick coronal brain sections at the
233 level of the lateral ventricles were cultured and immunofluorescence was performed using established

234 ependymal markers (Fig. 3A). Five days post electroporation, 77% of the McIdas-electroporated cells
235 expressed *P73*, as opposed to 13% of the GFP-electroporated cells, suggesting that astrocytes that
236 replaced damaged ependymal cells in LPA treated hydrocephalic mouse models acquired the ependymal
237 fate (Fig. 3B).

238 As ependymal cells normally require approximately two weeks until they acquire their mature
239 characteristics *in vivo*, we followed differentiation of electroporated cells at later time points and
240 examined whether they differentiate into fully mature multiciliated cells. Towards this direction, we
241 performed immunolabeling experiments making use of antibodies recognizing Pericentrin to mark basal
242 bodies and acetylated-a-tubulin to detect cilia (Fig. 3C). Nine days post electroporation 67% of McIdas
243 electroporated cells carried multiple basal bodies (Fig. 3D), while 16% of McIdas-electroporated cells
244 carried multiple cilia as revealed by acetylated-a-tubulin immunostaining (Fig. 3E). Basal bodies
245 amplification or multiple cilia formation was not detected in any of the control cells, electroporated with
246 a GFP expressing plasmid.

247 Collectively, our data show that *McIdas* forced expression in brain periventricular cells has the potential
248 to regenerate the ependymal cells in a mouse model of intracranial hemorrhage hydrocephalus.

249

250 **McIdas promotes *in vivo* reprogramming towards functional ependymal cells in a model of**
251 **congenital hydrocephalus**

252 We have recently described that genetic mutations in the human and mouse *GemC1* gene lead to
253 hydrocephalus (Lalioti *et al*, 2019b). Moreover, we have shown that radial glial cells lacking functional
254 *GemC1* fail to commit to the ependymal lineage and therefore do not develop ependymal cells during
255 embryogenesis. We took advantage of the *GemC1*-knockout genetic mouse model of hydrocephalus we

256 have generated to investigate whether reprogramming towards the ependymal cells could be achieved in
257 a model of congenital hydrocephalus.

258 We initially examined whether *McIdas* could program radial glial cells derived from *GemC1*-knockout
259 hydrocephalic mice into ependymal cells *ex vivo*. Postnatal radial glial cells isolated from *GemC1*-
260 knockout mice were infected with lentiviruses expressing either a GFP-McIdas (McIdas) fusion protein
261 or GFP as a control. Infected cells were analyzed at different time points for the expression of known
262 ependymal markers by immunofluorescence experiments, using specific antibodies recognizing FOXJ1,
263 Pericentrin and acetylated-a-tubulin proteins (Fig. EV4A). At five days post infection, 86% of the
264 McIdas-infected cells expressed *FoxJ1* and showed accumulation of multiple basal bodies, based on
265 Pericentrin immunostaining (Fig. EV4B, C). Moreover, our analysis revealed that 97% of the McIdas
266 transduced cells were multiciliated 15 days following infection, based on acetylated-a-tubulin and
267 Pericentrin staining (Fig. EV3D, E). By contrast, in GFP transduced cells neither *FoxJ1* expression nor
268 multiple basal bodies and cilia were observed. In addition, similar experiments were performed by
269 ectopically expressing *P73* in postnatal radial glial cells isolated from *GemC1*-knockout mice. Ectopic
270 expression of *P73* was not sufficient to induce *FoxJ1* expression nor multiple basal bodies or multiple
271 cilia formation in *GemC1*-knockout radial glial cells (Fig. EV4A-E). These results show that cells
272 derived from a genetic model of hydrocephalus can be programmed *ex vivo* into multiciliated ependymal
273 cells.

274 In order to examine whether *McIdas* promotes cellular reprogramming towards the ependymal cell
275 lineage *in vivo*, we have used our genetic mouse model of hydrocephalus which was previously
276 established (Lalioti *et al*, 2019b). Plasmid vectors encoding *McIdas* in conjunction with GFP or GFP
277 alone were electroporated into one lateral ventricle of newborn *GemC1*-knockout mouse brains targeting

278 periventricular cells which could be either neural progenitor cells or reactive astrocytes that have
279 replaced the lost ependymal cell population (Roales-Buján *et al*, 2012; Gonzalez-Cano *et al*, 2016; Abdi
280 *et al*, 2018; Lalioti *et al*, 2019b). Reprogramming towards the ependymal cells was evaluated through
281 immunofluorescence, using molecular markers that determine different stages of ependymogenesis.
282 Interestingly, four days post electroporation 61% and 58% of *McIdas*-electroporated cells were
283 immunopositive for the ependymal markers *P73* (Fig. 4A, B) and *FoxJ1*, respectively (Fig. EV5A, B).
284 The expression of *P73* and *FoxJ1* was not detected in control animals, in agreement to what was
285 previously described (Lalioti *et al*, 2019b), as *GemC1*-knockout mice lack ependymal cells. We also
286 showed that *McIdas* further promoted the differentiation of the electroporated ependymal cells as basal
287 bodies amplification was observed, based on Pericentrin immunofluorescence (Fig. 4C). More
288 specifically, upon *McIdas* overexpression 44% of the electroporated cells acquired multiple basal bodies
289 (Fig. 4D). In addition, immunofluorescence against acetylated-a-tubulin revealed that *McIdas*
290 overexpression resulted in the formation of cilia in a significant number of cells, corresponding to 7% of
291 *McIdas* electroporated cells (Fig. 4E). Noticeably, ciliated cells were located close to the ventricles,
292 resembling normal mature multiciliated ependymal cells, which form a single-layered ciliated
293 epithelium adjacent to the brain ventricle.

294 In order to examine whether the cilia that were generated upon *McIdas* ectopic expression were motile,
295 thick coronal brain sections from *GemC1*-knockout mice covering the lateral brain ventricles were
296 obtained and used in live imaging microscopy experiments (Fig. 5A). Electroporated cells were
297 identified under a FITC filter and their cilia beating capacity was examined in fast video records. A
298 proportion of cells with multiple beating cilia that were GFP-negative in sections derived from *McIdas*-
299 electroporated brains were observed. We have previously shown that *GemC1*-knockout mice are unable
300 to generate ependymal cells (Lalioti *et al*, 2019b), therefore cells carrying multiple beating cilia that do

301 not appear GFP-positive were possibly observed due to the loss of the transgene because of its transient
302 expression and were thus undetectable under the FITC filter. In addition to this, we cannot exclude the
303 possibility of dilution of the GFP signal due to continued proliferation. In agreement with what was
304 previously described cilia were not detected in brain sections following GFP overexpression. However,
305 McIdas electroporated cells exhibited functional beating cilia (Fig. 5B and Movies EV5, 6).
306 Kymographs were generated (Fig. 5C) following previously described methods by Francis et al. (Francis
307 & Lo, 2013) and ciliary beating frequency of McIdas induced ependymal cells was estimated to have a
308 mean value of 10 Hz (Fig. 5D).

309 Our findings show that McIdas induces ependymal cells restoration in the diseased hydrocephalic brain.

310

311 **McIdas expression contributes to the restoration of the subventricular zone niche cytoarchitecture**
312 **in hydrocephalic mice.**

313 The adult subventricular zone niche has a well-defined architecture formed by pinwheel-like structures.
314 These structures are assembled by the large apical domain of ependymal cells which surround the
315 smaller apical domain of adult neural stem cells (aNCSs) and constitute a unique micro-environment for
316 coordinating adult neurogenesis (Mirzadeh *et al*, 2008; Paez-Gonzalez *et al*, 2011; Kokovay *et al*, 2012).
317 To assess whether McIdas is able to restore the subventricular zone niche's cytoarchitecture in
318 hydrocephalic mice, whole-mount immunofluorescence was performed on ventricular walls of the
319 lateral ventricles of GemC1-knockout hydrocephalic mice at P7-P9, previously electroporated with an
320 *McIdas*-expressing plasmid or GFP alone. Specific antibodies against VCAM1 and GFAP, both markers
321 of aNCSs, and β -catenin to delineate cell boundaries were used. Our analysis showed that McIdas-
322 electroporated cells had a larger apical surface compared to control GFP-electroporated cells, which is

323 characteristic for multiciliated ependymal cells. In addition, McIdas-electroporated cells were
324 surrounding VCAM1- (Fig. 6A) and GFAP-immunopositive cells (Fig. 6B) reminiscent of pinwheel
325 structures. On the contrary, control GFP-electroporated cells had a small apical surface and pinwheel
326 structures were not detectable as it was previously described (Lalioti *et al*, 2019b). We also quantified
327 the number of electroporated cells that were detected in pinwheel structures, revealing that 18% of
328 McIdas-expressing cells were able to form pinwheel structures as opposed to GFP-electroporated cells
329 that were not detected in pinwheels (Fig. 6C). Our data suggest that McIdas expression is sufficient to
330 instruct the regeneration of ependymal cells in hydrocephalic mice which have the potential to re-build
331 the lost architecture of the subventricular zone niche.

332

333

334 **DISCUSSION**

335 During mammalian brain development neural progenitor cells transition from an uncommitted to a
336 restricted state, through a process that is influenced by lineage-specific gene expression programs,
337 resulting to terminally differentiated cells. Reprogramming allows the conversion of differentiated cells
338 from one lineage to another type of differentiated cell. Efficient reprogramming is highly dependent on
339 the selection of pioneer factors related to the desired cell type. Here, we demonstrate that GEMC1 and
340 MCIDAS, members of the geminin family, constitute potent reprogramming factors towards the
341 ependymal fate both *ex vivo* and *in vivo*.

342 *GemC1* and *McIdas* drive the cell fate commitment of a subpopulation of brain radial glial cells towards
343 multiciliated ependymal cells by coordinating gene expression of essential factors for ependymal cell
344 differentiation (Kyrousi *et al*, 2015). In addition, we have recently provided evidence that *GemC1*

345 expression is necessary and sufficient to establish the appropriate chromatin organization at multiple loci
346 for ependymal cells differentiation (Lalioti *et al*, 2019b). In light of this evidence, we hypothesized that
347 *GemC1* and *McIdas* could promote direct reprogramming towards the ependymal lineage in different
348 cellular populations under physiology and disease. We initially demonstrated that both *GemC1* and
349 *McIdas* overexpression were able to trigger the differentiation of mESCs into ependymal cells, as
350 evidenced by the upregulation of key factors of ependymogenesis and the generation of multiple cilia in
351 the *GemC1*- and *McIdas* overexpressing cells. We also showed that *GemC1* and *McIdas* overexpression
352 induce the expression of *P73* and *FoxJ1*, two well-established transcription factors of the molecular
353 pathway of multiciliogenesis, in cultured cortical astrocytes. Importantly, we demonstrated that *GemC1*
354 and *McIdas* activate the ependymal fate and induce the formation of multiple basal bodies and cilia in
355 the reprogrammed cells. The ectopic expression of *GemC1* resulted in a lower percentage of cells with
356 multiple basal bodies, a unique structural feature of ependymal cells, revealing a differential
357 reprogramming potential of the two factors. We showed that *GemC1* does not induce sufficient levels of
358 *McIdas* expression, that could contribute to the reduced ability of *GemC1* to execute as efficiently the
359 ependymal differentiation program. Moreover, using video microscopy experiments we showed that
360 *McIdas* ectopic expression was sufficient to reprogram cortical astrocytes into fully functional
361 multiciliated ependymal cells, as reprogrammed cells possessed multiple beating cilia that were able to
362 beat in a co-ordinated way and generate fluid flow. In addition, *McIdas* overexpression was sufficient to
363 induce the ependymal fate in radial glial cells derived from the brain of hydrocephalic mice in great
364 contrast to *P73*, further highlighting *McIdas*' ability to induce the ependymal cell fate. The stem cell
365 properties of the mESCs and radial glial cells used in our study are likely to facilitate the adoption of the
366 ependymal fate. Since this aligns with their differentiation spectrum their conversion to ependyma could
367 be considered as differentiation into the ependymal cell lineage.

368 It has been shown that in human and experimental hydrocephalus, disrupted ependyma is replaced by
369 astroglial cells (Sival *et al*, 2011; Roales-Buján *et al*, 2012; Guerra *et al*, 2015; McAllister, James P. *et*
370 *al*, 2017). This astrocytic scarring along the denuded ventricular wall contributes to the pathophysiology
371 of the disease as astrocytes do not restore ependymal functions; as they do not display cilia, produce
372 appropriate trophic signals, or facilitate the production of neurons (Sival *et al*, 2011; Roales-Buján *et al*,
373 2012). Therefore, our strategy revealing the successful conversion of isolated cortical astrocytes into
374 ependymal cells is of particular importance for treatment of hydrocephalus.

375 To investigate whether *McIdas* would also reprogram cells *in vivo*, we used a mouse model of
376 congenital hydrocephalus in which *GemC1* has been inactivated, and a model of acquired
377 hydrocephalus, triggered by intracranial hemorrhage. It was previously shown that *GemC1* deficiency in
378 mice results in the loss of the ependymal cells due to failure on activating the molecular program for the
379 cell fate commitment towards the ependymal lineage (Terré *et al*, 2016; Lalioti *et al*, 2019b). Moreover,
380 *GemC1* deficiency has been recently associated with congenital hydrocephalus in both humans and mice
381 (Lalioti *et al*, 2019b). In this study, we showed that *McIdas* forced expression induces the upregulation
382 of *P73* and *FoxJ1* in brain periventricular cells, which are likely to be neural progenitor cells or/and
383 reactive astrocytes that have replaced the ependymal cell population in the hydrocephalic brain. The
384 activation of the *P73* and *FoxJ1* genes uncovered the ability of *McIdas* to promote the initial steps of the
385 ependymal cell's differentiation program in the hydrocephalic brain. We also showed that *McIdas*-
386 overexpressing cells generated multiple basal bodies and cilia, both of which are unique features of
387 mature multiciliated ependymal cells, thus revealing the successful reprogramming towards ependyma.
388 Importantly, the multiple cilia of the reprogrammed cells presented functional activity, as we were able
389 to detect beating cilia upon *in vivo* overexpression of *McIdas* in the hydrocephalic mice. Using the LPA-
390 induced intracranial hydrocephalus mouse model, we demonstrated *McIdas* ability to convert

391 periventricular cells into ependymal cells. Previous study has shown that LPA causes substantial
392 depletion of the ependymal monolayer, loss of ependymal cilia and subsequent ependymal apoptotic cell
393 death (Lummis *et al*, 2019). In line with these findings, we did not observe multiciliated ependymal cells
394 in periventricular regions after LPA treatment. Instead, we observed GFAP-positive cells, likely reactive
395 astrocytes, covering the lateral ventricle walls where ependymal cells typically reside under normal
396 conditions, as it has been previously shown in hydrocephalic mice (Páez *et al*, 2007; Roales-Buján *et al*,
397 2012). Therefore, it is highly likely that McIdas reprograms astrocytes into ependymal cells in LPA-
398 treated mice. However, we cannot rule out the possibility that McIdas might also enhance the survival of
399 a subset of ependymal cells resistant to LPA-induced apoptosis.

400 Collectively, in our experiments we employed diverse cellular systems and technical approaches,
401 including plasmid and lentiviral vectors, to induce the overexpression of McIdas and GemC1 suggesting
402 that both GemC1 and McIdas can induce the programming or reprogramming of different cellular
403 populations irrespectively of the cell system and vector used. While our approach in the genetic mouse
404 model of hydrocephalus and the LPA-induced intracranial hydrocephalus likely targets periventricular
405 cells, which are neural progenitor cells or/and reactive astrocytes, we cannot rule out the possibility that
406 other cellular populations might also be targeted. Recent evidence from reprogramming experiments in
407 the mouse retina and the brain indicates that the insert sequences of overexpression constructs can alter
408 the specificity of the construct's promoter, introducing a bias toward the initial cell population being
409 targeted (Wang *et al*, 2021; Le *et al*, 2022). Additionally, future genetic lineage analysis using
410 transgenic mice to label neural progenitors and/or astrocytes would be needed to clarify which cell
411 population is differentiated into ependymal cells in our approach. One of the major clinical features in
412 human patients with hydrocephalus is the ventricular zone disruption phenomenon, characterized by the
413 loss of neural stem cells and ependyma (McAllister, James P. *et al*, 2017). Of note, sustained neuron

414 generation depends on the maintenance of the proper cytoarchitecture of the Ventricular-Subventricular
415 Zone (V-SVZ) niche of the brain, which requires preserving the structure of the ependymal cell
416 monolayer intact (Paez-Gonzalez *et al*, 2011). In the present study, we targeted V-SVZ-resident cells in
417 the hydrocephalic brain in which *McIdas* overexpression was induced and observed that McIdas-
418 overexpressing cells populated areas of the ventricular zone niche next to the lateral ventricles, where
419 ependymal cells normally reside under homeostasis. We have used SVZ electroporation to target the
420 periventricular cells of one lateral ventricle of the hydrocephalic brain of GemC1-knockout mice, which
421 results to a limited number of electroporated cells. Therefore, following this experimental approach, the
422 small number of ependymal cells which is generated is not possible to contribute to a significant
423 reduction in the volume of the lateral ventricles as a readout of resolved or reduced hydrocephalus. It has
424 been described that disruption of the ventricular/subventricular zone (V/SVZ) is a critical and consistent
425 factor in the pathophysiology of hydrocephalus (McAllister, James P. *et al*, 2017; Jiménez *et al*, 2014).
426 In our study we showed that McIdas ectopic expression contributes to the restoration of the lost
427 cytoarchitecture of the niche in hydrocephalic mice, as we identified reprogrammed ependymal cells
428 forming pinwheel-like structures with resident neural stem cells in the targeted ventricular wall. Our
429 findings suggest that McIdas forced expression in human patients with hydrocephalus would contribute
430 to the re-establishment of the SVZ niche leading to brain functions' improvement by enhancing neuronal
431 production in human patients with hydrocephalus and ameliorating brain function. The *in vivo*
432 reprogramming approach indicates that the in-situ conversion of cells into ependyma in its native
433 microenvironment is feasible. Our *in vivo* approach allowed the exploration of the influence of the
434 diseased environment of the hydrocephalic brain on the reprogramming process. Our data support the
435 idea that functional maturation and integration of the reprogrammed cells in the native tissue can be
436 achieved through our *in vivo* reprogramming method. Since the molecular program of multiciliogenesis

437 is conserved across different organisms and tissues (Arbi *et al*, 2018), it is tempting to speculate that
438 such a reprogramming approach could be applied to other diseases that impact ciliated tissues, such as
439 the lung and the reproductive system. For instance, a rare genetic disorder affecting the mucociliary
440 clearance mechanism, known as Reduced Generation of Multiple Motile Cilia (RGMC), has been linked
441 to mutations in MCIDAS. Therefore, it would be highly interesting to investigate whether these
442 conditions could be addressed in the future through a genetic treatment implementing McIdas'
443 overexpression in the affected tissue.

444 Together, our analysis proposes MCIDAS and GEMC1 as potent reprogramming factors towards the
445 ependymal cell lineage and demonstrate a proof of concept that restoring ependymal cells could
446 contribute in managing hydrocephalus. Although the present study yielded intriguing findings, our
447 implementation holds certain limitations. In particular, our *in vivo* studies have been conducted to mouse
448 models of hydrocephalus. Despite sharing a similar pathophysiology with the human disease, the
449 anatomical and physiological characteristics of the mouse and human brain possess certain differences.
450 Therefore, to validate the effectiveness of our approach, additional experiments in disease models closer
451 to human pathophysiology will be required. The pig model demonstrates anatomical and physiological
452 similarities to humans and replicates the pathophysiology of human hydrocephalus, exhibiting features
453 such as ventriculomegaly, V/SVZ disruption, and neuroinflammation and could thus be a valuable
454 model for examining the translational success of our approach to the human conditions (Garcia-Bonilla
455 *et al*, 2023). Additionally, since hydrocephalus in our study appeared during early developmental stages,
456 our findings are particularly relevant to postnatal hydrocephalus. Therefore, their applicability to adult
457 hydrocephalus will require further investigation using appropriate adult animal models. Although we
458 achieved McIdas overexpression in the periventricular cells of the diseased brain through
459 electroporation, such an approach cannot be used in humans. Therefore, alternative gene delivery

460 methods compatible with therapeutic protocols, such as AAV gene delivery strategies in the human
461 brain (Chamakioti *et al*, 2022; Au *et al*, 2022) should be established. Our study shows that regeneration
462 of multiciliated ependymal cells can be succeeded in hydrocephalic mouse models while further
463 experiments are needed to show the applicability of our findings in treating hydrocephalus in humans.

464

465 METHODS

466 Mouse knockout strain

467 C57/Bl6 mice carrying a knockout (KO) allele of the *GemC1* gene were initially generated by the trans-
468 NIH Knock-Out Mouse Project (KOMP) and obtained from the KOMP repository. The *GemC1*-KO
469 allele was maintained on a mixed strain background. Inactivation of the *GemC1* gene was carried out
470 using the “knockout-first” strategy, as previously described (Arbi *et al*, 2016; Lalioti *et al*, 2019b). This
471 approach involves disrupting gene function by adding RNA processing signals without removing any of
472 the targeted genes (Testa *et al*, 2004). The *GemC1*-KO allele was created by placing a lacZ-neo cassette
473 between the second and third exon of the gene.

474 Mice were housed in the animal house of the University of Patras, where a standard light cycle of 12
475 hours of light and 12 hours of darkness was maintained. Continuous access to food and water was
476 ensured at all times. To ensure animal welfare handling and environmental stressors like noise,
477 vibrations, and strong odors were minimized to necessary levels. All animal-related procedures were
478 conducted in strict accordance with EU directives and approved by the Veterinary Administrations of
479 the Prefecture of Achaia, Greece, and the Research Ethics Committee of the University of Patras,
480 Greece.

481 In all experiments, mice were used without regard to their gender. Experiments involving animal usage
482 were conducted during the neonatal stage when the gender of the animals was not yet
483 distinguishable.**LPA preparation and injections**

484 To generate an inducible mouse model of intracranial-hemorrhage hydrocephalus, we performed
485 intraventricular delivery of lysophosphatidic acid (LPA) in wild-type (WT) mice at postnatal day five
486 (P5), following previously published works (Yung *et al*, 2011; Lummis *et al*, 2019).

487 Powdered 18:1 LPA (857130P, Avanti Polar Lipids) was initially dissolved in methanol and
488 subsequently vacuum-dried. LPA was then reconstituted in Hanks' balanced salt solution (HBSS 14065-
489 049, Gibco) by sonicating in a water bath for 5 min to generate a 10 mM stock, as previously described
490 (Yung *et al*, 2011; Lummis *et al*, 2019). Stock solution was stored at -20°C until use. Using a glass
491 microcapillary, 3 µl of the 10 mM LPA stock solution together with Fast Green (0.1%, Sigma) were
492 injected into the lateral ventricle of P5 mice upon hypothermia-anesthetization. Mice were sacrificed
493 two days post LPA injections at P7 and were examined or further processed as described in the
494 respective experiments.

495 **Plasmid constructs**

496 For neonatal electroporation and mESCs transfection experiments mouse cDNAs for McIdas and
497 GemC1 were cloned in pCAGGS-IRES-GFP vectors between SacI/EcoRV and NheI/SmaI restriction
498 sites respectively, as described previously (Kyrousi *et al*, 2015).

499 **Neonatal electroporation**

500 Neonatal electroporation was performed at P0-P1. Anesthesia was induced via hypothermia. Using a
501 pulled glass microcapillary, 2 µg plasmid DNA together with Fast Green (0.1%, Sigma) were injected in
502 the lateral ventricle of the mouse brains. Mice were subsequently electroporated with 5 pulses of 100V
503 for 50ms each followed by intervals of 950ms. An ECM830 Electroporator (Harvard Apparatus) and 7
504 mm platinum electrodes (BTX) were used. Following electroporation mice were placed back to cages
505 and left to grow for 4 or 6-14 days before sacrificed as described in the respective experiments.

506 ***Ex vivo* electroporation and organotypic brain slice cultures**

507 For *ex vivo* electroporation, mice were sacrificed 2 days post LPA-injections at P7. Mouse brains were
508 dissected and placed in cold DMEM/F-12 medium (Gibco). Subsequently, 2 µg plasmid DNA of a
509 pCAGGS-IRES-GFP (GFP) or pCAGGS-McIdas-IRES-GFP (McIdas) vector together with Fast Green
510 (0.1%, Sigma) were injected in the lateral ventricle using a pulled glass microcapillary. Brains were then

511 electroporated with 5 pulses applied at 100V for 50ms each at intervals of 950ms. An ECM830
512 Electroporator (Harvard Apparatus) and 7 mm platinum electrodes (BTX) were used.

513 For organotypic brain slice cultures 250 μ m thick coronal slices were obtained from the electroporated
514 brains using a vibrating microtome (Leica VT1000 S). Consecutive slices containing the lateral
515 ventricles were collected and placed in culturing medium [2% FBS (Gibco), 1% GlutaMAX Supplement
516 (Gibco) and 1% Penicillin-Streptomycin (Gibco) in DMEM/F-12]. Subsequently, brain slices were
517 placed onto 0.4 μ m membrane inserts (Millipore) in 6-well plates and cultured for 5 or 9 days in
518 culturing medium, performing medium change every three days.

519 **Lentiviral production**

520 A second generation packaging system was used to generate lentiviral expression particles as previously
521 described (Arbi *et al*, 2016). The pLV-Dest-CAG lentiviral expression vector was used and was kindly
522 provided by Dr. M. Gotz, Helmholtz Center, Munich. The cloning strategy for generating the lentiviral
523 expression vectors for GFP and GemC1 with an N-terminal GFP tag (GFP-GemC1) was described
524 elsewhere (Arbi *et al*, 2016).

525 McIdas with an N-terminal GFP tag (GFP-McIdas) was initially cloned into the KpnI/XhoI restriction
526 sites of the pENTR1AminusCmR vector. p73 with a C-terminal GFP tag (p73-GFP) was initially cloned
527 into the SalI/NotI restriction sites of the pENTR1AminusCmR vector. An LR recombination reaction,
528 using the Gateway LR Clonase II enzyme mix (Invitrogen), was performed between the attL-containing
529 entry clone and the attR-containing destination pLVDest-CAG vector.

530 **Primary cultures of postnatal cortical astroglia and lentiviral infection**

531 To establish primary cultures of postnatal cortical astroglia, the cerebral cortex of postnatal P5-P7 wild-
532 type mice was dissected from the brain. Cells were subsequently mechanically dissociated and cultured
533 under proliferating conditions for 7 days in astro medium containing DMEM/F-12 (Gibco), 10% FBS
534 (Gibco), 2% B27 Supplement (Gibco), 1% GlutaMAX Supplement (Gibco), 1% Penicillin-Streptomycin
535 (Gibco), epidermal growth factor (10ng/ml) and basic fibroblast growth factor (10ng/ml), as previously
536 described (Heinrich *et al*, 2011).

537 For lentiviral infection, astroglial cells were plated onto poly-D-lysine pre-coated coverslips 7 days upon
538 proliferation initiation and were left to attach and grow for 2-4 hours. Cells were then transduced with
539 concentrated lentiviral vectors. The infection mix was removed 24 hours later and was replaced by astro
540 medium which did not contain FBS, epidermal growth factor and basic fibroblast growth factor to favor
541 differentiation. Cells were analyzed 7 and 14 days later.

542 **Primary cultures of postnatal radial glial cells and lentiviral infection**

543 To establish primary cultures of postnatal radial glial cells (pRGCs), the lateral walls of the lateral
544 ventricles of P0-P1 mice were dissected, mechanically dissociated, and then plated onto poly-D-lysine
545 pre-coated coverslips. pRGCs were cultured in proliferation medium [DMEM-high glucose (Gibco),
546 10% FBS (Gibco), and 1% penicillin/streptomycin (Gibco)] for three days (Paez-Gonzalez *et al*, 2011;
547 Kyrousi *et al*, 2015; Lalioti *et al*, 2019b). Subsequently, pRGCs were infected with unconcentrated viral
548 particles performing plate-spin infection. Proliferation medium was changed 24 hours post-infection and
549 later replaced with differentiation medium [DMEM-high glucose (Gibco), 2% FBS (Gibco), and 1%
550 penicillin/streptomycin (Gibco)] 48 hours post-infection. Cells were processed for analysis 5 or 15 days
551 upon differentiation initiation.

552 **Cultures of mouse embryonic stem cells (mESCs) and transfection**

553 Mouse embryonic stem cells were grown onto gelatin-coated (0.1% gelatin, Sigma) flasks in GMEM
554 BHK-21 medium (Gibco), supplemented with 10% FBS (Biosera, Embryonic Stem Cells tested), 0.1
555 mM β -mercaptoethanol (Gibco), 2 mM L-glutamine (Sigma), 1 mM sodium pyruvate (Pan Biotech), 1%
556 penicillin/streptomycin (Gibco), 1% MEM Non-Essential Amino Acids (Biosera) and 2.000 U/ml LIF
557 (Millipore). Cells were passaged every other day and were mycoplasma tested.

558 Reverse mESCs transfection was performed using the jet-OPTIMUS reagent according to
559 manufacturer's instructions. Briefly, the transfection mixes containing DNA, jet-OPTIMUS buffer and
560 transfection reagent were prepared. Afterwards, transfection mixes were placed on gelatin pre-coated
561 glass coverslips and then mESCs were immediately seeded. Cells were cultured in the presence of LIF
562 for 24 hours. The following day the medium was changed (LIF withdrawal), and the cells were cultured
563 in differentiating conditions for up to 6 days and were then processed for analysis.

564 **Video microscopy of ependymal cilia**

565 For the study of ependymal cilia in primary cultures of reprogrammed postnatal cortical astroglia, cells
566 were grown under proliferating conditions in astro medium for 7 days. Cells were then plated onto poly-
567 D-lysine coated glass-bottom dishes (ibidi) and transduced with unconcentrated lentiviral vectors. 24
568 hours post infection, medium was replaced by astro medium which did not contain FBS, epidermal
569 growth factor and basic fibroblast growth factor to favor differentiation. Cells were used in video
570 microscopy experiments 22 days later.

571 To perform video microscopy experiments in reprogrammed postnatal cortical astroglia, the culturing
572 medium was replaced by live imaging medium containing MEM (Sigma), 20% FBS (Gibco), 4 mM L-
573 glutamine (Sigma) and 1 mM sodium pyruvate (Pan Biotech). In addition, to track cilia generated fluid
574 flow 0.5 μ m red fluorescent microbeads (1 μ l/ml medium; Sigma) were added to the imaging medium.
575 Video microscopy experiments were performed using an Olympus IX83 microscope equipped with a
576 Hamamatsu Orca-Flash 4.0 sCMOS camera. During live imaging microscopy experiments cells were
577 maintained at 37°C and 5% CO₂. Videos were obtained using a 60x water immersion objective at 80
578 frames/sec, while 500 frames were acquired for each field.

579 For the study of brain ependymal cilia, mice were sacrificed at P7-P15, brains were dissected in HBSS
580 at room temperature and 200 μ m thick coronal slices were obtained using a vibrating microtome. Slices
581 containing the lateral ventricles were placed in DMEM-GlutaMAX (Gibco) media pre-warmed at 37°C.

582 To perform video microscopy experiments, brain slices were placed onto glass-bottom dishes containing
583 live imaging medium with 0.5 μ m red fluorescent microbeads (1 μ l/ml medium). Video recordings were
584 obtained as described in the preceding paragraph.

585 For cilia beat frequency analysis, the ImageJ image processing program was used to firstly generate a
586 graphical representation of cilia beating, in the form of a kymograph, as previously described by
587 Drummond I. (Drummond, 2009). Cilia beat frequency for each multiciliated cell was then calculated
588 with the correlation of the time scale of the video recording with the kymograph, following the method
589 described by Francis R. and Lo C. (Francis & Lo, 2013).

590 To track the trajectory of the moving microbeads the MTrackJ Plugin of the ImageJ program was used.
591 In short, the point selection tool was used to manually mark the position of each red fluorescent

592 microbead in each frame. Consecutive marks on the corresponding video recordings created the
593 trajectory of the microbeads.

594 **Whole-mount dissection**

595 SVZ whole mounts were obtained as previously described (Lalioti *et al*, 2019b). Briefly, the brain was
596 isolated and the electroporated lateral ventricle was carefully separated from the posterior region of the
597 telencephalon, followed by the extraction of the hippocampus and septum. Fixation of the dissected
598 lateral wall was performed in 4% PFA/0.1% Triton X-100 at 4°C overnight. Staining was then
599 performed (see below, immunofluorescence) and the lateral wall was further dissected from the
600 surrounding brain parenchyma, resulting in tissue slivers with a thickness of 200-300 micrometers.
601 These slivers were then affixed to a glass slide using Mowiol 4-88 (Calbiochem) mounting media and
602 covered with a coverslip.

603

604 **Immunofluorescence**

605 For immunofluorescence, cultured cells were fixed for 10 min with 4% PFA (or 10 min PFA 4%
606 followed by 10 min fixation in Methanol where stated) and incubated in blocking solution, for 1hr at
607 room temperature. Postnatal cortical astroglial cells were incubated in blocking solution containing 5%
608 FBS, 3% BSA, 0.1% Triton X-100 in 1× PBS. pRGCs and mESCs were incubated in blocking solution
609 containing 5% Normal Goat Serum (Jackson Immunoresearch) and 0.3% Triton-X100 in 1x PBS. Cells
610 were incubated with primary antibodies in blocking solution at 4°C, overnight (Kalogeropoulou *et al*,
611 2022).

612 Brains dissected from newborn mice (up to P7) were fixed overnight with 4% PFA. Subsequently,
613 brains were rinsed with 1x PBS and cryopreserved with incubation in 30% sucrose in 1x PBS for ~48
614 hours. Brains were then frozen in 7.5% gelatin supplemented with 15% sucrose and sectioned at 12 µm
615 using a CM1850 Leica cryostat. Brain coronal cryosections were postfixed with 4% PFA for 10 min,
616 treated with 0.3% Triton X-100 in 1× PBS for 5 min, and incubated in blocking solution containing 5%
617 FBS, 3% BSA, 0.1% Triton X-100 in 1× PBS, for 1-3 hrs. Samples were incubated with primary
618 antibodies in blocking solution at 4°C, overnight.

619 For immunofluorescence of cultured brain slices, membrane inserts were removed, rinsed in 1x PBS and
620 fixed with 4% PFA at 4°C, overnight. Membrane inserts were then subjected to consecutive washes in
621 1x PBS (5 min), 0.1% Triton X-100 in 1× PBS (5 min) and 0.5% Triton X-100 in 1× PBS (20 min once)
622 and were incubated in blocking solution containing 1% FBS, 0.1% Triton X-100 in 1× PBS for 2-3 hrs
623 at room temperature. Samples were incubated with primary antibodies in blocking solution at 4°C,
624 overnight.

625 Immunofluorescence of SVZ whole-mounts was performed as previously described (Mirzadeh *et al*,
626 2008, 2010). Briefly, whole-mounts were incubated for 1-2 hrs at room temperature in blocking
627 solution, containing 10% normal goat serum in 0.1 M PBS with 0.5-2% Triton-X100. Samples were
628 incubated with primary antibodies in blocking solution at 4°C for 24-48 hrs.

629 The following primary antibodies were used: chicken anti-GFP (1020, Aves Laboratories, 1:500 for
630 brain sections; 1:1000 for cells, 1:250 for whole mounts), mouse anti-S100 β (S2532, Sigma, 1:250),
631 rabbit anti-P73 (ab40658, Abcam, 1:300), mouse anti-FoxJ1 (14-9965, eBioscience, 1:500), rabbit anti-
632 pericentrin (PRB432C, Covance, 1:750 for brain sections; 1:1500 for cells), rabbit anti-GFAP (Z0334,
633 DakoCytomation, 1:1000 for cells, 1:500 for whole-mounts), mouse anti-acetylated α -tubulin (T6793,
634 Sigma, 1:1000 for brain sections; 1:1500 for cells), rabbit anti-McIdas ((Pefani *et al*, 2011), 1:250),
635 mouse anti-centriolin (sc-365521, Santa Cruz, 1:100, cells' fixation in PFA-Methanol), rabbit anti-
636 Meig1 (orb185566, Biorbyt, 1:100), rat anti-VCAM1 (550547, BD Biosciences, 1:100), mouse anti β -
637 catenin (610153, BD Biosciences, 1:500), guinea pig anti-double-cortin (AB2253, Millipore, 1:500).

638 The following Alexa Fluor-labeled secondary antibodies (Invitrogen) were used in the respective
639 blocking solution (1:1000) for 1 hr (cryosections and cells) at room temperature or overnight (membrane
640 inserts) at 4°C: Alexa Fluor 488 goat anti-chicken, Alexa Fluor 568 goat anti-mouse IgG1, Alexa Fluor
641 647 donkey anti-rabbit, Alexa Fluor 568 goat anti-rabbit, Alexa Fluor 647 goat anti-mouse IgG1, Alexa
642 Fluor 568 goat anti-mouse, Alexa Fluor 568 goat anti-rabbit, Alexa Fluor 647 donkey anti-mouse, Alexa
643 Fluor 568 goat anti-guinea pig and Alexa Fluor 568 goat anti-rat. DNA was stained either with Draq-5
644 (1:1000, Biostatus) or Dapi (1:1500, Sigma). Samples were mounted in Mowiol 4-88 (Calbiochem).

645 **Microscopy and data analysis**

646 Images of fluorescent samples were acquired with a confocal Leica TCS SP5 and a Leica TCS SP8
647 system equipped with a fluorescent Leica DMI600B or Leica DMi8 microscope, respectively. 20x, 40x
648 and 63x lenses were used. Digital images were processed with Adobe Photoshop and the ImageJ image
649 processing program. For still images related to video microscopy experiments, individual frames were
650 cropped and adjusted for brightness and contrast in ImageJ.

651 Quantification of cells on overexpressed brains from in vivo experiments was performed on
652 cryosections, vibratome sections or whole-mounts. In all instances, each brain region containing
653 electroporated cells was imaged and quantified per frame. All quantifications are expressed as
654 percentages of the total cell count. Quantification of radial glial cells, cortical astrocytes, or mESCs from
655 ex-vivo experiments was performed in at least two independent experiments, with a minimum of 15
656 different images analyzed for each condition in each experiment. Fluorescent intensity per nucleus was
657 measured using the open-source platform ImageJ.

658 The number of independent experiments performed for each analysis is mentioned in the corresponding
659 figure legend. Normality was tested for each experiment using the Shapiro-Wilk test to determine if the
660 sample data came from a normally distributed population. Since our data did not follow a normal
661 distribution, statistical analysis was performed with the non-parametric two-tailed Mann–Whitney test.
662 Significant differences in medians were determined by p value: P<0.05 (*P<0.05, **P<0.01,
663 ***P<0.001). Each graph displayed the median ± interquartile range (IQR). All statistical analyses and
664 graph preparation were performed in GraphPad Prism 6.

665 The study did not incorporate blinding or randomization, and all samples were included without
666 applying specific inclusion or exclusion criteria. These choices were guided by the exploratory nature of
667 the research.**DATA AVAILABILITY**

668 This study includes no data deposited in external repositories.

669

670 **ACKNOWLEDGMENTS**

671 We thank the Advanced Light Microscopy Facility of the Medical School at the University of Patras and
672 the Experimental Animal Facility of the University of Patras for support with experiments. We are also
673 grateful to Andriana Charalampopoulou and members from Professor's Benedikt Berninger laboratory
674 for their assistance in astrocytic reprogramming experiments. We also thank Dr. Christina Kyrousi and
675 members of our laboratories for helpful discussions and Nikolaos Giakoumakis for his assistance with
676 whole-mount images processing. This study was supported by the Hellenic Foundation for Research and
677 Innovation (H.F.R.I.) under the "2nd Call for H.F.R.I. Research Projects to support Faculty Members &
678 Researchers" (Project Number: 2735), the Hydrocephalus Association USA and Fondation Santé to S.T.,
679 and the State Scholarships Foundation (IKY) to K.K.

680

681 **DISCLOSURE AND COMPETING INTERESTS STATEMENT**

682 | Zoi Lygerou is an EMBO Council member. This has no bearing on the editorial consideration of this
683 article for publication.

684 **THE PAPER EXPLAINED:**

685 Medical issue

686 Hydrocephalus is a condition where fluid builds up in the brain cavities, leading to serious health issues.
687 Standard treatment involves surgery, which is risky and often fails over time. Ependymal cells have
688 multiple tiny hair-like structures (cilia) on their surface to circulate the fluid, and their impairment may
689 lead to hydrocephalus.

690 Results

691 We showed that GemC1 and McIdas, which are known regulators of multiciliated ependymal cell fate
692 determination, can instruct different cell types to differentiate into ependymal cells. We further managed
693 to convert brain cells of hydrocephalic animal models into ependymal cells.

694 Clinical impact

695 Our findings suggest new therapeutic intervention aiming at the regeneration of damaged ependymal
696 cells in human hydrocephalus. .

697

698

699 **REFERENCES**

- 700 Abdi K, Lai C-H, Paez-Gonzalez P, Lay M, Pyun J & Kuo CT (2018) Uncovering inherent cellular
701 plasticity of multiciliated ependyma leading to ventricular wall transformation and
702 hydrocephalus. *Nat Commun* 9: 1655
- 703 Arbi M, Pefani D, Kyrousi C, Lalioti M, Kalogeropoulou A, Papanastasiou AD, Taraviras S & Lygerou
704 Z (2016) GemC1 controls multiciliogenesis in the airway epithelium. *EMBO Rep* 17: 400–413
- 705 Arbi M, Pefani D-E, Taraviras S & Lygerou Z (2018) Controlling centriole numbers: Geminin family
706 members as master regulators of centriole amplification and multiciliogenesis. *Chromosoma*
707 127: 151–174
- 708 Au HKE, Isalan M & Mielcarek M (2022) Gene Therapy Advances: A Meta-Analysis of AAV Usage in
709 Clinical Settings. *Frontiers in Medicine* 8
- 710 Bocchi R, Masserdotti G & Götz M (2022) Direct neuronal reprogramming: Fast forward from new
711 concepts toward therapeutic approaches. *Neuron* 110: 366–393
- 712 Boon M, Wallmeier J, Ma L, Loges NT, Jaspers M, Olbrich H, Dougherty GW, Raidt J, Werner C,
713 Amirav I, et al (2014) MCIDAS mutations result in a mucociliary clearance disorder with
714 reduced generation of multiple motile cilia. *Nat Commun* 5: 4418
- 715 Chamakioti M, Karantzelis N & Taraviras S (2022) Advanced Gene-Targeting Therapies for Motor
716 Neuron Diseases and Muscular Dystrophies. *International Journal of Molecular Sciences* 23:
717 4824
- 718 Drummond I (2009) Studying cilia in zebrafish. *Methods Cell Biol* 93: 197–217
- 719 Francis R & Lo C (2013) Ex vivo method for high resolution imaging of cilia motility in rodent airway
720 epithelia. *J Vis Exp*
- 721 Funk MC, Bera AN, Menchen T, Kuales G, Thriene K, Lienkamp SS, Dengjel J, Omran H, Frank M &
722 Arnold SJ (2015) Cyclin O (Ccno) functions during deuterosome-mediated centriole
723 amplification of multiciliated cells. *EMBO J* 34: 1078–1089
- 724 Garcia-Bonilla M, Nair A, Moore J, Castaneyra-Ruiz L, Zwick SH, Dilger RN, Fleming SA, Golden
725 RK, Talcott MR, Isaacs AM, et al (2023) Impaired neurogenesis with reactive astrocytosis in the
726 hippocampus in a porcine model of acquired hydrocephalus. *Experimental Neurology* 363:
727 114354

- 728 Gonzalez-Cano L, Fuertes-Alvarez S, Robledinos-Anton N, Bizy A, Villena-Cortes A, Fariñas I,
729 Marques MM & Marin MC (2016) p73 is required for ependymal cell maturation and neurogenic
730 SVZ cytoarchitecture: p73 Regulates SVZ Cytoarchitecture. *Developmental Neurobiology* 76:
731 730–747
- 732 Guerra MM, Henzi R, Ortloff A, Lichtin N, Vío K, Jiménez AJ, Dominguez-Pinos MD, González C,
733 Jara MC, Hinostroza F, *et al* (2015) Cell Junction Pathology of Neural Stem Cells Is Associated
734 With Ventricular Zone Disruption, Hydrocephalus, and Abnormal Neurogenesis. *J Neuropathol
735 Exp Neurol* 74: 653–671
- 736 Heinrich C, Gascón S, Masserdotti G, Lepier A, Sanchez R, Simon-Ebert T, Schroeder T, Götz M &
737 Berninger B (2011) Generation of subtype-specific neurons from postnatal astroglia of the mouse
738 cerebral cortex. *Nat Protoc* 6: 214–228
- 739 Ji W, Tang Z, Chen Y, Wang C, Tan C, Liao J, Tong L & Xiao G (2022) Ependymal Cilia: Physiology
740 and Role in Hydrocephalus. *Frontiers in Molecular Neuroscience* 15
- 741 Jiménez AJ, Domínguez-Pinos M-D, Guerra MM, Fernández-Llebrez P & Pérez-Fígares J-M (2014)
742 Structure and function of the ependymal barrier and diseases associated with ependyma
743 disruption. *Tissue Barriers* 2: e28426
- 744 Kahle KT, Kulkarni AV, Limbrick DD & Warf BC (2016) Hydrocephalus in children. *The Lancet* 387:
745 788–799
- 746 Kalogeropoulou A, Mougkogianni M, Iliadou M, Nikolopoulou E, Flordelis S, Kanellou A, Arbi M,
747 Nikou S, Nieminuszczy J, Niedzwiedz W, *et al* (2022) Intrinsic neural stem cell properties define
748 brain hypersensitivity to genotoxic stress. *Stem Cell Reports* 17: 1395–1410
- 749 Kokovay E, Wang Y, Kusek G, Wurster R, Lederman P, Lowry N, Shen Q & Temple S (2012) VCAM1
750 is essential to maintain the structure of the SVZ niche and acts as an environmental sensor to
751 regulate SVZ lineage progression. *Cell Stem Cell* 11: 220–230
- 752 Kousi M & Katsanis N (2016) The Genetic Basis of Hydrocephalus. *Annu Rev Neurosci* 39: 409–435
- 753 Kyrousi C, Arbi M, Pilz G-A, Pefani D-E, Lalioti M-E, Ninkovic J, Götz M, Lygerou Z & Taraviras S
754 (2015) Mcidas and GemC1 are key regulators for the generation of multiciliated ependymal cells
755 in the adult neurogenic niche. *Development* 142: 3661–3674
- 756 Kyrousi C, Lygerou Z & Taraviras S (2017) How a radial glial cell decides to become a multiciliated
757 ependymal cell. *Glia* 65: 1032–1042
- 758 Lalioti M-E, Arbi M, Loukas I, Kaplani K, Kalogeropoulou A, Lokka G, Kyrousi C, Mizi A,
759 Georgomanolis T, Josipovic N, *et al* (2019a) GemC1 governs multiciliogenesis through direct
760 interaction with and transcriptional regulation of p73. *J Cell Sci* 132

- 761 Lalioti M-E, Kaplani K, Lokka G, Georgomanolis T, Kyrousi C, Dong W, Dunbar A, Parlapani E,
762 Damianidou E, Spassky N, *et al* (2019b) GemC1 is a critical switch for neural stem cell
763 generation in the postnatal brain. *Glia*
- 764 Le N, Appel H, Pannullo N, Hoang T & Blackshaw S (2022) Ectopic insert-dependent neuronal
765 expression of GFAP promoter-driven AAV constructs in adult mouse retina. *Front Cell Dev Biol*
766 10
- 767 Lim DA, Tramontin AD, Trevejo JM, Herrera DG, García-Verdugo JM & Alvarez-Buylla A (2000)
768 Noggin Antagonizes BMP Signaling to Create a Niche for Adult Neurogenesis. *Neuron* 28: 713–
769 726
- 770 Lummis NC, Sánchez-Pavón P, Kennedy G, Frantz AJ, Kihara Y, Blaho VA & Chun J (2019) LPA1/3
771 overactivation induces neonatal posthemorrhagic hydrocephalus through ependymal loss and
772 ciliary dysfunction. *Sci Adv* 5: eaax2011
- 773 Ma L, Quigley I, Omran H & Kintner C (2014) Multicilin drives centriole biogenesis via E2f proteins.
774 *Genes Dev* 28: 1461–1471
- 775 MacDonald A, Lu B, Caron M, Caporicci-Dinucci N, Hatrock D, Petrecca K, Bourque G & Stratton JA
776 (2021) Single Cell Transcriptomics of Ependymal Cells Across Age, Region and Species
777 Reveals Cilia-Related and Metal Ion Regulatory Roles as Major Conserved Ependymal Cell
778 Functions. *Front Cell Neurosci* 15
- 779 Marshall CB, Mays DJ, Beeler JS, Rosenbluth JM, Boyd KL, Santos Guasch GL, Shaver TM, Tang LJ,
780 Liu Q, Shyr Y, *et al* (2016) p73 Is Required for Multiciliogenesis and Regulates the Foxj1-
781 Associated Gene Network. *Cell Reports* 14: 2289–2300
- 782 McAllister, James P., Guerra, Maria Montserrat, Ruiz, Leandro Castaneyra, Jimenez, Antonio J.,
783 Dominguez-Pinos, Dolores, Sival, Deborah, den Dunnen, Wilfred, Morales, Diego M., Schmidt,
784 Robert E., Rodriguez, Esteban M., *et al* (2017) Ventricular Zone Disruption in Human Neonates
785 With Intraventricular Hemorrhage. *Journal of neuropathology and experimental neurology* 76:
786 358–375
- 787 Mirzadeh Z, Doetsch F, Sawamoto K, Wichterle H & Alvarez-Buylla A (2010) The subventricular zone
788 en-face: wholemount staining and ependymal flow. *J Vis Exp*: 1938
- 789 Mirzadeh Z, Merkle FT, Soriano-Navarro M, Garcia-Verdugo JM & Alvarez-Buylla A (2008) Neural
790 Stem Cells Confer Unique Pinwheel Architecture to the Ventricular Surface in Neurogenic
791 Regions of the Adult Brain. *Cell Stem Cell* 3: 265–278
- 792 Nemajerova A, Kramer D, Siller SS, Herr C, Shomroni O, Pena T, Suazo CG, Glaser K, Wildung M,
793 Steffen H, *et al* (2016) TAp73 is a central transcriptional regulator of airway multiciliogenesis.
794 *Genes Dev*

- 795 Páez P, Bátiz L-F, Roales-Buján R, Rodríguez-Pérez L-M, Rodríguez S, Jiménez AJ, Rodríguez EM &
796 Pérez-Fígares JM (2007) Patterned neuropathologic events occurring in hyh congenital
797 hydrocephalic mutant mice. *J Neuropathol Exp Neurol* 66: 1082–1092
- 798 Paez-Gonzalez P, Abdi K, Luciano D, Liu Y, Soriano-Navarro M, Rawlins E, Bennett V, Garcia-
799 Verdugo JM & Kuo CT (2011) Ank3-Dependent SVZ Niche Assembly Is Required for the
800 Continued Production of New Neurons. *Neuron* 71: 61–75
- 801 Rekate HL (2009) A Contemporary Definition and Classification of Hydrocephalus. *Seminars in*
802 *Pediatric Neurology* 16: 9–15
- 803 Roales-Buján R, Páez P, Guerra M, Rodríguez S, Vío K, Ho-Plagaro A, García-Bonilla M, Rodríguez-
804 Pérez L-M, Domínguez-Pinos M-D, Rodríguez E-M, et al (2012) Astrocytes acquire
805 morphological and functional characteristics of ependymal cells following disruption of
806 ependyma in hydrocephalus. *Acta Neuropathol* 124: 531–546
- 807 Rodríguez EM & Guerra MM (2017) Neural Stem Cells and Fetal-Onset Hydrocephalus. *Pediatr*
808 *Neurosurg* 52: 446–461
- 809 Sawamoto K, Wichterle H, Gonzalez-Perez O, Cholfin JA, Yamada M, Spassky N, Murcia NS, Garcia-
810 Verdugo JM, Marin O, Rubenstein JLR, et al (2006) New neurons follow the flow of
811 cerebrospinal fluid in the adult brain. *Science* 311: 629–632
- 812 Schrandt-Stumpel C & Fryns JP (1998) Congenital hydrocephalus: nosology and guidelines for clinical
813 approach and genetic counselling. *Eur J Pediatr* 157: 355–362
- 814 Sival DA, Guerra M, den Dunnen WFA, Bátiz LF, Alvial G, Castañeyra-Perdomo A & Rodríguez EM
815 (2011) Neuroependymal denudation is in progress in full-term human foetal spina bifida aperta.
816 *Brain Pathol* 21: 163–179
- 817 Stubbs JL, Vladar EK, Axelrod JD & Kintner C (2012) Multicilin promotes centriole assembly and
818 ciliogenesis during multiciliate cell differentiation. *Nat Cell Biol* 14: 140–147
- 819 Tan FE, Vladar EK, Ma L, Fuentealba LC, Hoh R, Espinoza FH, Axelrod JD, Alvarez-Buylla A, Stearns
820 T, Kintner C, et al (2013) Myb promotes centriole amplification and later steps of the
821 multiciliogenesis program. *Development* 140: 4277–4286
- 822 Terré B, Piergiovanni G, Segura-Bayona S, Gil-Gómez G, Youssef SA, Attolini CS-O, Wilsch-
823 Bräuninger M, Jung C, Rojas AM, Marjanović M, et al (2016) GEMC1 is a critical regulator of
824 multiciliated cell differentiation. *EMBO J* 35: 942–960
- 825 Testa G, Schaft J, van der Hoeven F, Glaser S, Anastassiadis K, Zhang Y, Hermann T, Stremmel W &
826 Stewart AF (2004) A reliable lacZ expression reporter cassette for multipurpose, knockout-first
827 alleles. *Genesis* 38: 151–158

828 Wallmeier J, Al-Mutairi DA, Chen C-T, Loges NT, Pennekamp P, Menchen T, Ma L, Shamseldin HE,
829 Olbrich H, Dougherty GW, *et al* (2014) Mutations in CCNO result in congenital mucociliary
830 clearance disorder with reduced generation of multiple motile cilia. *Nat Genet* 46: 646–651

831 Wang L-L, Serrano C, Zhong X, Ma S, Zou Y & Zhang C-L (2021) Revisiting astrocyte to neuron
832 conversion with lineage tracing in vivo. *Cell* 184: 5465-5481.e16

833 Yung YC, Mutoh T, Lin M, Noguchi K, Rivera RR, Choi JW, Kingsbury MA & Chun J (2011)
834 Lysophosphatidic Acid Signaling May Initiate Fetal Hydrocephalus. *Sci Transl Med* 3: 99ra87

835 Yung YC, Stoddard NC, Mirendil H & Chun J (2015) Lysophosphatidic acid (LPA) signaling in the
836 nervous system. *Neuron* 85: 669–682

837

838

839 **FIGURE LEGENDS**

840 Figure 1.

841 **McIdas forced expression promotes *ex vivo* reprogramming of murine cortical astrocytes into
842 ependymal cells.**

843 (A) Schematic representation of experimental procedures for (B-G). Astrocytes were isolated from the
844 cortex of neonatal mice and were cultured under proliferating conditions. Subsequently, cells were
845 transduced with lentiviral vectors encoding GFP or GFP-McIdas (McIdas) and cultured under
846 differentiating conditions for indicated time points.

847 (B) Cortical astrocytes were immunostained against GFP (green) to mark infected cells, P73 (grey) and
848 S100 β (red) at day 7 of differentiation. Arrows point to McIdas-infected cells which are P73+ and
849 represent cells committed to the ependymal lineage.

850 (C-D) The graph depicts the percentage of the infected cells that co-express the ependymal marker P73
851 over the total number of the infected cells (C) The percentage of the infected cells which display S100 β
852 staining around their cell body, which corresponds to ependymal cells, is depicted in the graph (D) Data
853 are presented as the median \pm interquartile range (IQR) of three independent experiments. Statistical
854 significance was determined using the non-parametric two-tailed Mann–Whitney test (**p < 0.0001).

855 (E) Transduced astrocytes were immunostained at differentiation day 14 against GFP (green), FoxJ1
856 (grey) and pericentrin (PCNT, red). Note the presence of multiple basal bodies, based on PCNT signal
857 accumulation, in McIdas-infected cells which co-express the ependymal marker FoxJ1 (arrows).

858 (F-G) The graphs present the percentage of the infected cells that express FoxJ1 over the total number of
859 the infected cells (F) and the percentage of FoxJ1-positive infected cells which also display
860 accumulation of PCNT signal (G). Data are presented as the median \pm IQR of three independent
861 experiments. Statistical significance was determined using the non-parametric two-tailed Mann–
862 Whitney test (**p < 0.0001).

863 DNA was stained with Dapi (blue). Scale bars, 10 μ m.

864 Abbreviations, dd: differentiation day

865

866 Figure 2.

867 **McIdas reprograms cortical astrocytes into functional ependymal cells.**

868 (A) Immunofluorescence of transduced cortical astrocytes at differentiation day 22 with antibodies
869 against GFP (green), Glial Fibrillary Acidic Protein (GFAP, grey) which labels astrocytes and acetylated
870 a-tubulin (ACT, red), a marker of ciliary axonemes. McIdas expression triggers the formation of
871 multiple cilia, tiny hair-like structures which appear on the surface of the reprogrammed astrocytes
872 (arrow). Note the downregulation of the GFAP signal in the reprogrammed multiciliated cells. DNA was
873 stained with Dapi (blue). Scale bars, 10 μ m

874 (B-C) The graph shows the percentage of infected cells that express GFAP and correspond to an
875 astrocytic population (B) The percentage of the infected cells which possess multiple cilia based on
876 ACT staining is depicted in the graph (C) Data are presented as the median \pm IQR of two independent
877 experiments. Statistical significance was determined using the non-parametric two-tailed Mann–
878 Whitney test (**p < 0.0001).

879 (D) Live imaging microscopy experiments were performed on cortical astrocytes transduced either with
880 GFP or McIdas lentiviruses. The positions of fluorescent beads included in the live imaging medium,
881 were marked with colored dots on selected video frames. Track of one representative bead is shown in
882 the right panel. Two independent experiments were performed. Scale bar, 10 μ m

883 Abbreviations, dd: differentiation day

884

885 Figure 3.

886 **McIdas induces ependymal cells regeneration in a mouse model of intracranial hemorrhage**
887 **hydrocephalus.**

888 (A) Mice received unilateral intracranial injection of Lysophosphatidic acid (LPA) to induce
889 hydrocephalus. Coronal brain slices derived from brains electroporated either with a GFP or GFP-
890 McIdas (McIdas) plasmid were cultured for 5 days. Immunofluorescence experiments were performed
891 with antibodies against GFP (green) and the ependymal marker P73 (red). Inserts show higher
892 magnification images. Arrows indicate GFP+P73+ cells.
893 (B) The graph depicts the percentage of the electroporated cells that co-express the ependymal marker
894 P73, over the total number of the electroporated cells, at day 5 of culture. Data are presented as the
895 median \pm IQR of three independent experiments. Statistical significance was determined using the non-
896 parametric two-tailed Mann–Whitney test (**p = 0.0002).
897 (C) Coronal brain slices were cultured for 9 days and immunostained against GFP (green), pericentrin
898 (PCNT, red) and acetylated α -tubulin (ACT, grey) to detect mature multiciliated cells. Note the presence
899 of multiple basal bodies and cilia in McIdas electroporated cells.
900 (D-E) The percentage of the electroporated cells that carry multiple basal bodies, based on PCNT
901 accumulation signal, upon 9 days of culture, is presented in the graph (D), (**p < 0.0001). The graph
902 shows the percentage of multiciliated cells based on PCNT and ACT staining (E) upon 9 days of culture,
903 (p=0.0013). Data are presented as the median \pm IQR of three independent experiments. Statistical
904 significance was determined using the non-parametric two-tailed Mann–Whitney test.
905 DNA was stained with Dapi (blue). Scale bars, 10 μ m. .
906

907 Figure 4.

908 **McIdas ectopic expression promotes *in vivo* reprogramming into ependymal cells in a genetic
909 mouse model of hydrocephalus.**

910 (A) Neonatal subventricular zone electroporation was conducted at GemC1-knockout mice at postnatal
911 day 1 (P1) with plasmids encoding GFP, or GFP-McIdas (McIdas). Mice were sacrificed 4 days post
912 electroporation and coronal brain sections were immunostained with antibodies against GFP (green) and
913 P73 (red). Arrows point to McIdas-electroporated cells co-expressing P73, which represent cells
914 committed to the ependymal lineage. Higher magnification of the boxed region is shown in the right
915 panel.
916 (B) The graph shows the percentage of the electroporated cells expressing P73. Data are presented as the
917 median \pm IQR of three independent experiments. Statistical significance was determined using the non-
918 parametric two-tailed Mann–Whitney test (**p < 0.0001).

919 (C) Coronal brain sections from GemC1-knockout electroporated mice were stained with specific
920 antibodies against GFP (green), Pericentrin (PCNT, red) and acetylated a-tubulin (ACT grey). Multiple
921 basal bodies and cilia on the surface of McIdas electroporated cells are indicated by an arrow. Higher
922 magnification of the boxed region is shown in the right panel.

923 (D-E) Quantification of the percentage of the electroporated cells with multiple basal bodies, based on
924 PCNT accumulation (D), (** $p < 0.0001$), and the percentage of multiciliated cells based on PCNT and
925 ACT staining over the total number of the electroporated cells (E), ($P=0.0041$). Data are presented as the
926 median \pm IQR of two independent experiments. Statistical significance was determined using the non-
927 parametric two-tailed Mann–Whitney test.

928 DNA was stained with Dapi (blue). Scale bars, 10 μ m. .

929 Abbreviations, LV: lateral ventricle

930

931 Figure 5.

932 **McIdas establishes cilia motility in reprogrammed cells in a genetic mouse model of**
933 **hydrocephalus.**

934 (A) Schematic representation of experimental procedures for (B-D). GFP or GFP-McIdas (McIdas)
935 expressing plasmids were electroporated at the lateral ventricle of postnatal day 1 (P1) GemC1-knockout
936 mouse brains. Coronal brain sections, that contained the lateral ventricles, were obtained from the
937 electroporated mice at ages P7-P15 and were used in live imaging experiments.

938 (B) Cilia still images from GFP or McIdas electroporated brains at indicated time points in milliseconds.
939 FITC fluorescent cells are presented together with brightfield images. Arrows indicate the positions of
940 cilia at indicated time points. Cilia motility was observed upon McIdas ectopic expression as evidenced
941 by cilia changing positions at indicated time points. Higher magnification of the boxed regions is shown
942 in the right panels.

943 (C) Representative kymograms depicting cilia motility upon GFP or McIdas ectopic expression. Left
944 panel images show the lines used to obtain the kymograms. These images are extracted from the image
945 shown in B, which was utilized to generate the kymograph.(D) The graph shows cilia beat frequency of
946 electroporated cells quantified from high-speed brightfield cilia motility movies. Data are presented as
947 the median \pm IQR ($n=2$ for GFP (control) and $n=4$ for McIdas). Statistical significance was determined
948 using the non-parametric two-tailed Mann–Whitney test (** $p < 0.0001$).

949

950 Figure 6.

951 **Ectopic expression of McIdas restores the subventricular zone niche cytoarchitecture.**

952 (A-B) GemC1-knockout mouse brains were electroporated with plasmids encoding GFP or McIdas-GFP
953 (McIdas) at postnatal day 1 (P1). Mice were sacrificed at ages P7-P9 and lateral ventricular wall whole-
954 mount immunofluorescence was conducted with antibodies against GFP (green), β -catenin (red), and
955 Vascular Cell adhesion Molecule 1 (VCAM1, grey) (A) or Glial Fibrillary Acidic Protein (GFAP, grey)
956 (B).

957 Formation of pinwheel structures by McIdas-reprogrammed ependymal cells surrounding VCAM1+
958 neural stem cells (arrow, A) or GFAP-expressing neural stem cells (B) was observed. Note the enlarged
959 apical domain of McIdas-reprogrammed ependymal cells.

960 Higher magnification of the boxed region is shown in the right panel.

961 (C) The graph shows the percentage of electroporated cells, shown in A, identified in pinwheel
962 structures. Data are presented as the median \pm IQR (n=3 for GFP (control) and n=4 for McIdas).
963 Statistical significance was determined using the non-parametric two-tailed Mann–Whitney test (**p <
964 0.0001.).

965 Scale bars, 10 μ m.

966

967

968 EV Figure Legends

969

970 Figure EV1.

971 **Mouse embryonic stem cells programming into ependymal cells.**

972 (A) Mouse embryonic stem cells (mESCs) were transfected with GFP, GFP-McIdas (McIdas) or GFP-
973 GemC1 (GemC1) expressing vectors and subsequently cultured under differentiating conditions.
974 Immunofluorescence was performed with antibodies against GFP (green), FoxJ1 (red) and Pericentrin
975 (PCNT, magenta) at differentiation day 4. The arrow points to multiple basal bodies in McIdas and
976 GemC1 transfected cells which co-express the ependymal marker FoxJ1. Higher magnification of the
977 boxed regions is shown in the right panels.

978 (B-C) The graphs present the percentage of transfected mESCs that express FoxJ1 over the total number
979 of the transfected cells (B) and the percentage of transfected cells which display multiple basal bodies
980 based on the accumulation of PCNT signal (C) Data are presented as the median \pm IQR of two

981 independent experiments. Statistical significance was determined using the non-parametric two-tailed
982 Mann–Whitney test (**p < 0.0001).

983 (D) GFP (green), PCNT (magenta) and acetylated-a-tubulin (ACT red) immunostaining in transfected
984 mESCs at differentiation day 6. McIdas and GemC1 transfected mESCs present multiple basal bodies
985 and cilia.

986 (E) The graph shows the percentage of transfected cells with multiple basal bodies (PCNT
987 accumulation) and multiple cilia (ACT labeled cilia) over the total number of the transfected cells. Data
988 are presented as the median ±IQR of two independent experiments. Statistical significance was
989 determined using the non-parametric two-tailed Mann–Whitney test (**p < 0.0001).

990 DNA was stained with Dapi (blue). Scale bars, 10 µm,

991 Abbreviations, dd: differentiation day

992

993 Figure EV2.

994 **GemC1 drives the commitment of murine cortical astrocytes towards the ependymal cell lineage.**

995 (A) Cortical astrocytes were transduced with lentiviruses encoding GFP or GFP-GemC1 (GemC1).
996 Immunofluorescence experiments were performed at day 7 of differentiation with specific antibodies
997 against GFP (green) to mark the infected cells, P73 (grey) and S100 β (red). Arrow point to a P73+
998 infected cell, committed to the ependymal lineage.

999 (B-C) Graph depicting the percentage of infected cells which express P73 over the total number of
1000 infected cells (B). The graph shows the percentage of the infected cells which display S100 β staining
1001 around their cell body (C). Three independent experiments were analyzed. Data are presented as the
1002 median ±IQR. Statistical significance was determined using the non-parametric two-tailed Mann–
1003 Whitney test (**p < 0.0001).

1004 (D) Astrocytes were immunostained against GFP (green), FoxJ1 (grey) and pericentrin (PCNT red) at
1005 differentiation day 14. The arrow points to a GemC1-infected cell which expresses FoxJ1 and possesses
1006 multiple basal bodies.

1007 (E-F) Graph presenting the percentage of the infected cells that express FoxJ1 over the total number of
1008 the infected cells (E) The graph shows the percentage of infected cells which express the ependymal
1009 marker FoxJ1 and display accumulation of PCNT signal (F). Data are presented as the median ±IQR
1010 from three independent experiments. Statistical significance was determined using the non-parametric
1011 two-tailed Mann–Whitney test (**p < 0.0001).

1012 DNA was stained with Dapi (blue). Scale bars, 10 µm

1013 Abbreviations, dd: differentiation day

1014

1015 Figure EV3.

1016 **Lysophosphatidic Acid (LPA) administration causes hydrocephalus in early postnatal stages in**
1017 **mice.**

1018 (A) Top views of Postnatal day 7 (P7) wild type mouse brains that either received or not injection of
1019 LPA at the lateral ventricle at P5. No differences on the size of the brain were observed
1020 macroscopically.

1021 (B) Dapi staining on coronal brain sections from P7 mouse brains reveals the dilation of the lateral
1022 ventricles after LPA injections. Scale bar, 100 µm.

1023 (C) Immunofluorescence for Glial Fibrillary Acidic Protein (GFAP, green) which labels astrocytes and
1024 acetylated α-tubulin (ACT, red), a marker of ciliary axonemes on coronal sections from P7 mouse brains
1025 at the dorsal-lateral and lateral regions of the lateral walls. Arrowheads point to multiple cilia in control
1026 ependymal cells (ep). Arrows show GFAP positive astrocytes (as) in the lateral wall of LPA-injected
1027 brains, where ciliary disruption is observed. Higher magnification of the boxed regions is shown in the
1028 right panels. Scale bars, 10 µm

1029 DNA was stained with Dapi or Draq-5 (blue).

1030

1031 Figure EV4.

1032 ***Ex vivo* reprogramming of radial glial cells to ependyma can be achieved through McIdas ectopic**
1033 **expression.**

1034 (A) Schematic representation of experimental procedures for (B-E). Postnatal radial glial cells (pRGCs)
1035 were isolated from GemC1-knockout newborn mice, cultured and infected with lentiviruses expressing a
1036 GFP-McIdas (McIdas) or a GFP-P73 (P73) fusion protein, while GFP alone was used as a control. Cells
1037 were then cultured under differentiating conditions and analyzed at indicated timepoints.

1038 (B) Transduced radial glial cells were co-stained with antibodies against GFP (green) to mark infected
1039 cells, FoxJ1 (red) and pericentrin (PCNT, grey) 5 days after the initiation of differentiation. The arrow
1040 indicates the accumulation of PCNT signal in FoxJ1 expressing cells upon McIdas ectopic expression.

1041 (C) The graph presents the percentage of infected cells which express FoxJ1 and display multiple basal
1042 bodies (accumulation of PCNT signal). Three independent experiments were analyzed. Data are

1043 presented as the median \pm IQR. Statistical significance was determined using the non-parametric two-
1044 tailed Mann–Whitney test (** $p < 0.0001$).

1045 (D) Radial glial cells infected with GFP, McIdas, or P73 lentiviruses were labeled with antibodies
1046 against GFP (green), pericentrin (PCNT, grey) and acetylated a-tubulin (ACT, red) to detect mature
1047 multiciliated cells at differentiation day 15 (arrow).

1048 (E) The percentage of the infected cells which displayed multiple basal bodies, based on PCNT staining
1049 and simultaneously multiple cilia, based on ACT staining, was analyzed. Data are presented as the
1050 median \pm IQR of three independent experiments. Statistical significance was determined using the non-
1051 parametric two-tailed Mann–Whitney test (** $p < 0.0001$).

1052 DNA was stained with Hoechst (blue). Scale bars, 10 μ m.

1053

1054 Figure EV5.

1055 **McIdas drives the commitment to the ependymal cell lineage in a genetic mouse model for**
1056 **hydrocephalus.**

1057 (A) Subventricular zone electroporation was conducted at postnatal day 1 (P1) GemC1-knockout mice
1058 with plasmids encoding GFP, or GFP-McIdas (McIdas). Coronal brain sections were stained with
1059 antibodies against GFP (green) to mark the electroporated cells and FoxJ1 (red), a marker of committed
1060 ependymal cells, 4 days post electroporation. Arrows point to McIdas-electroporated cells expressing
1061 FoxJ1. Higher magnification of the boxed region is shown in the right panel.

1062 (B) Graph depicting the percentage of electroporated cells that express FoxJ1 over the total number of
1063 the electroporated cells. Two independent experiments were analyzed. Data are presented as the median
1064 \pm IQR. Statistical significance was determined using the non-parametric two-tailed Mann–Whitney test
1065 (** $p < 0.0001$).

1066 DNA was stained with Dapi (blue). Scale bars, 10 μ m

1067

1068

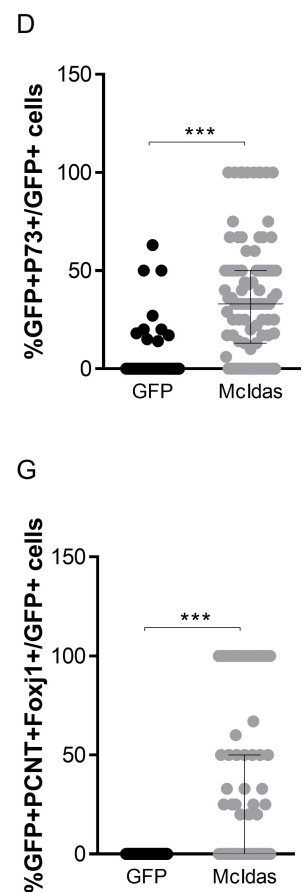
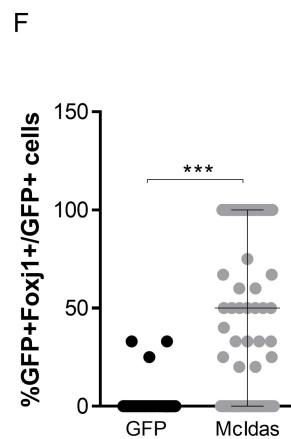
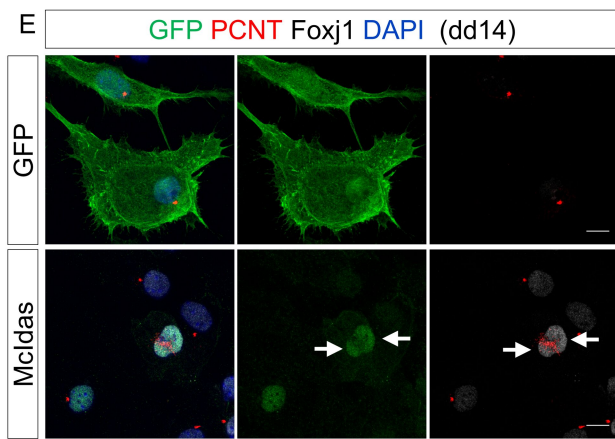
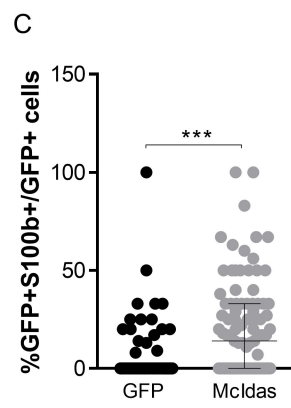
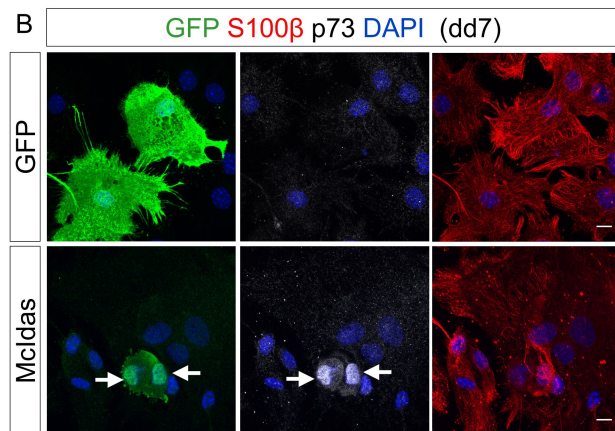
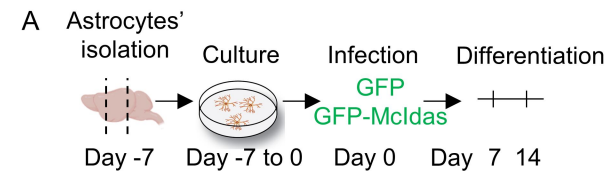
Figure 1

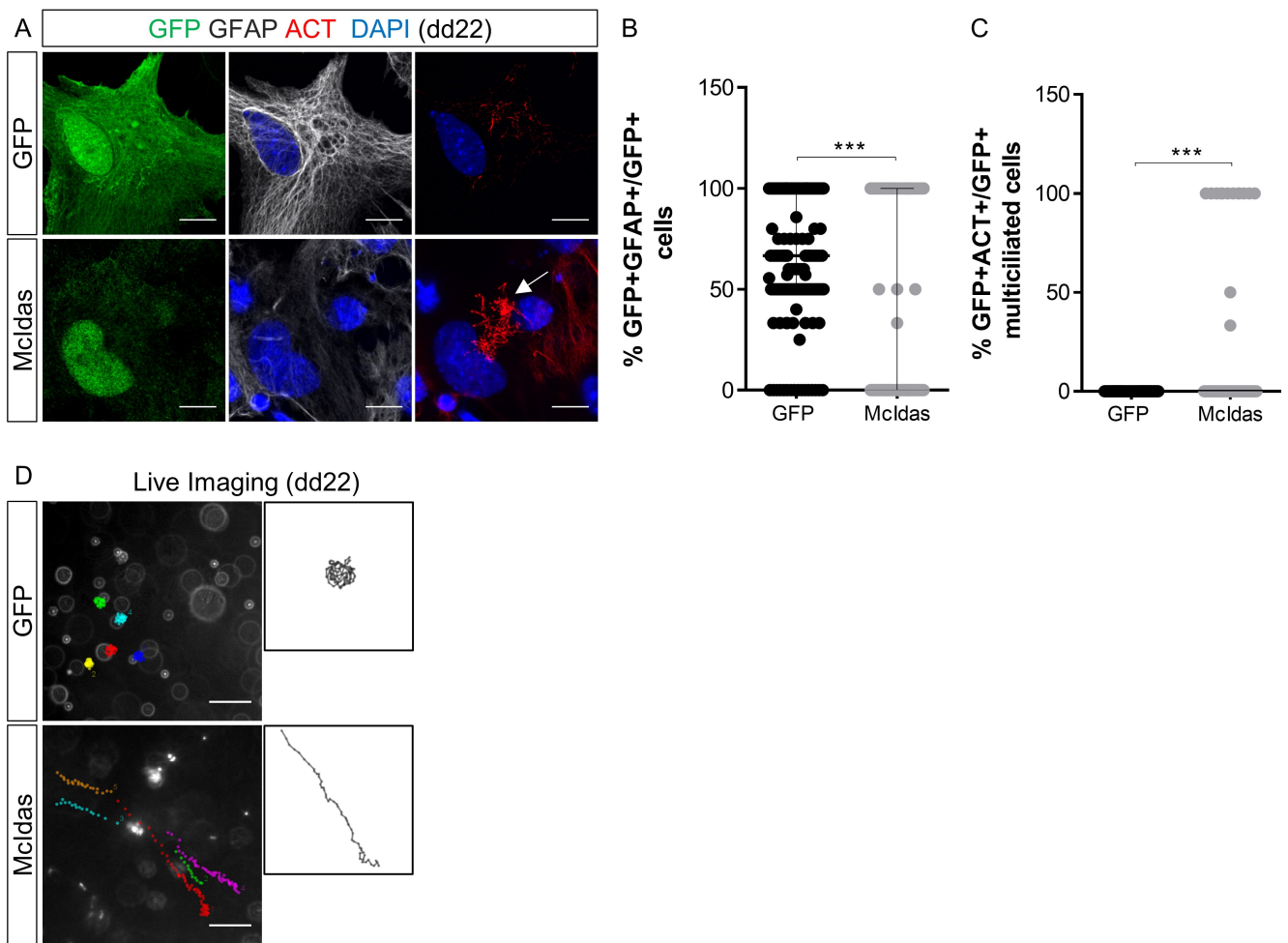
Figure 2

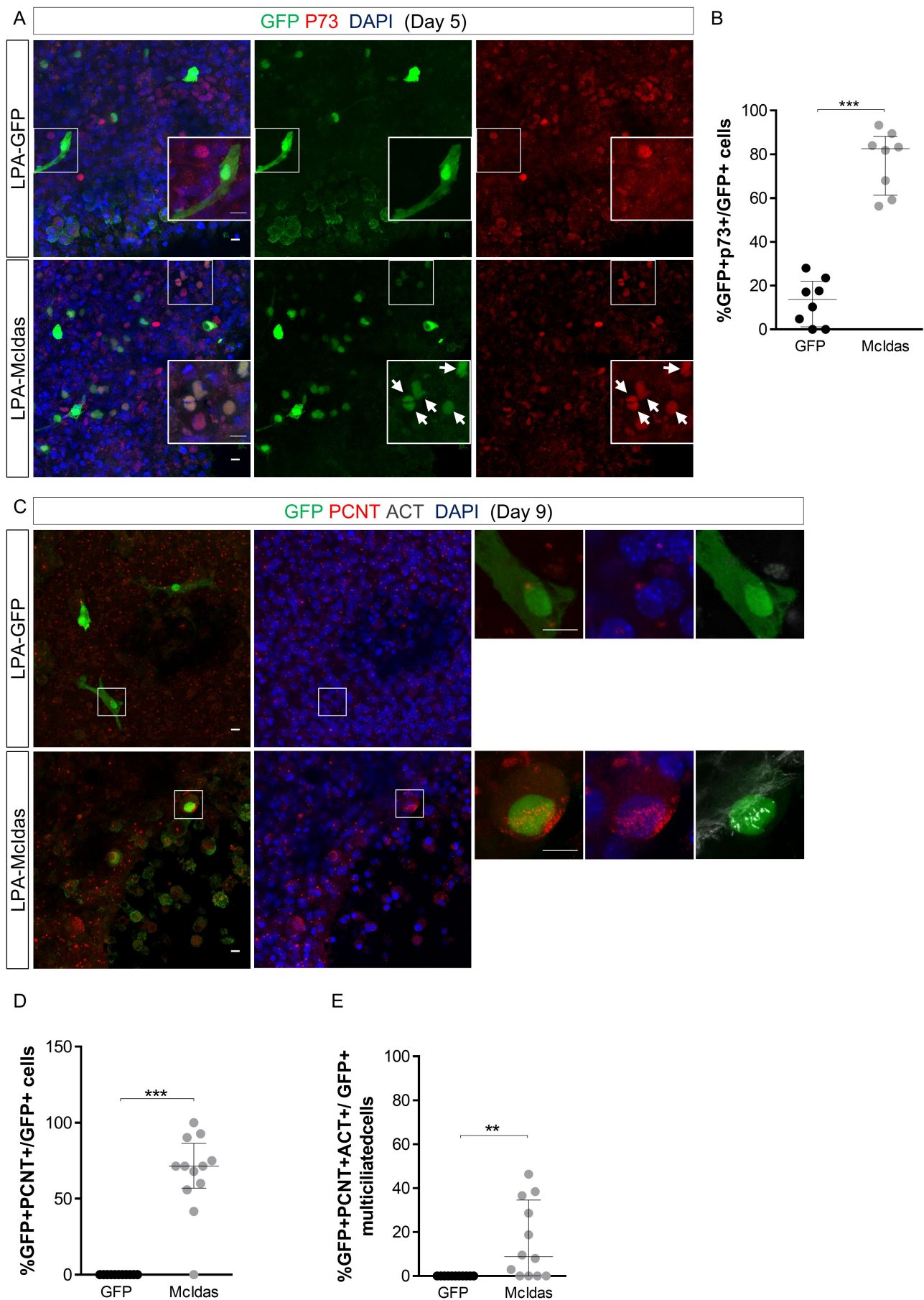
Figure 3

Figure 4

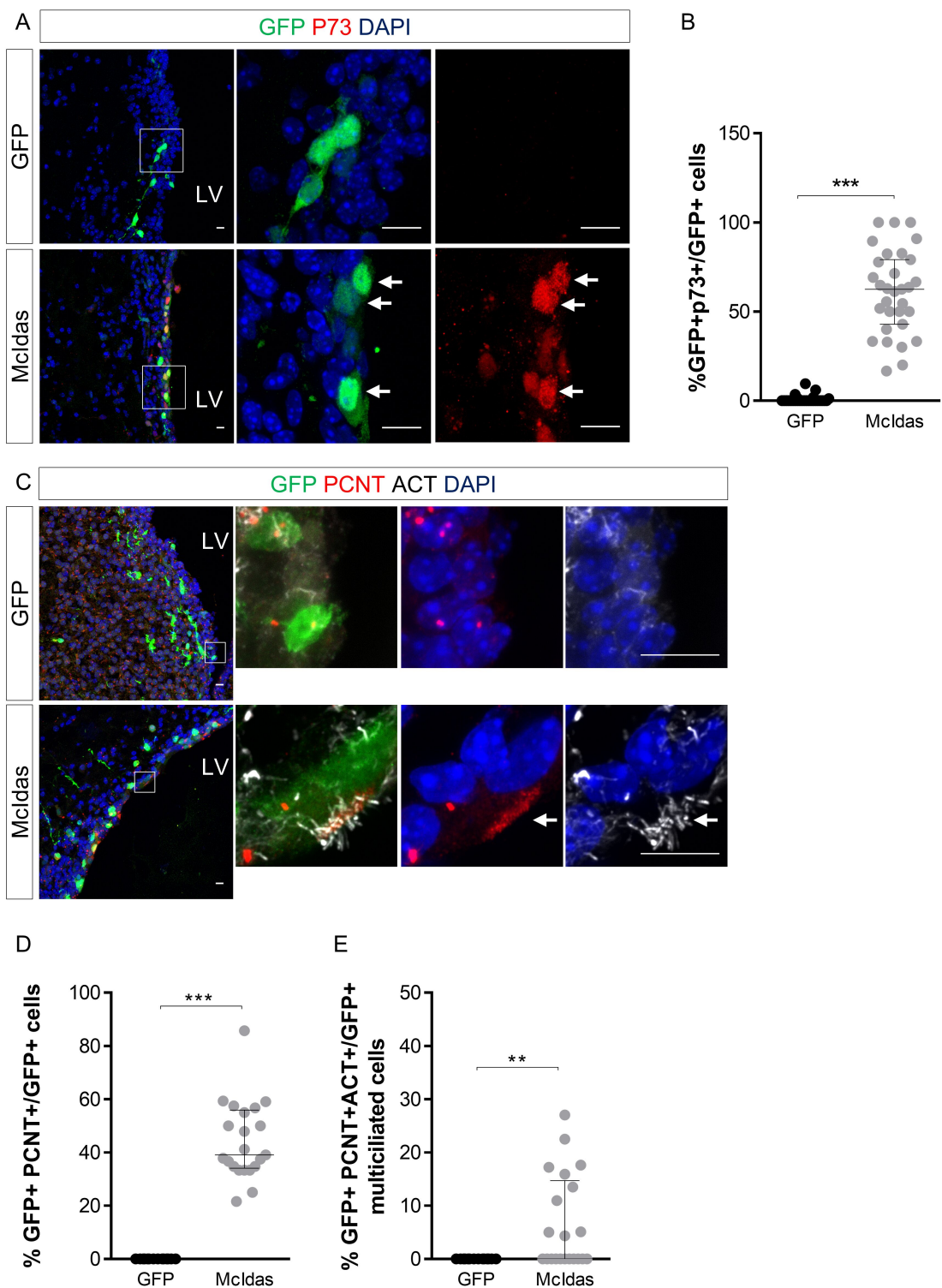


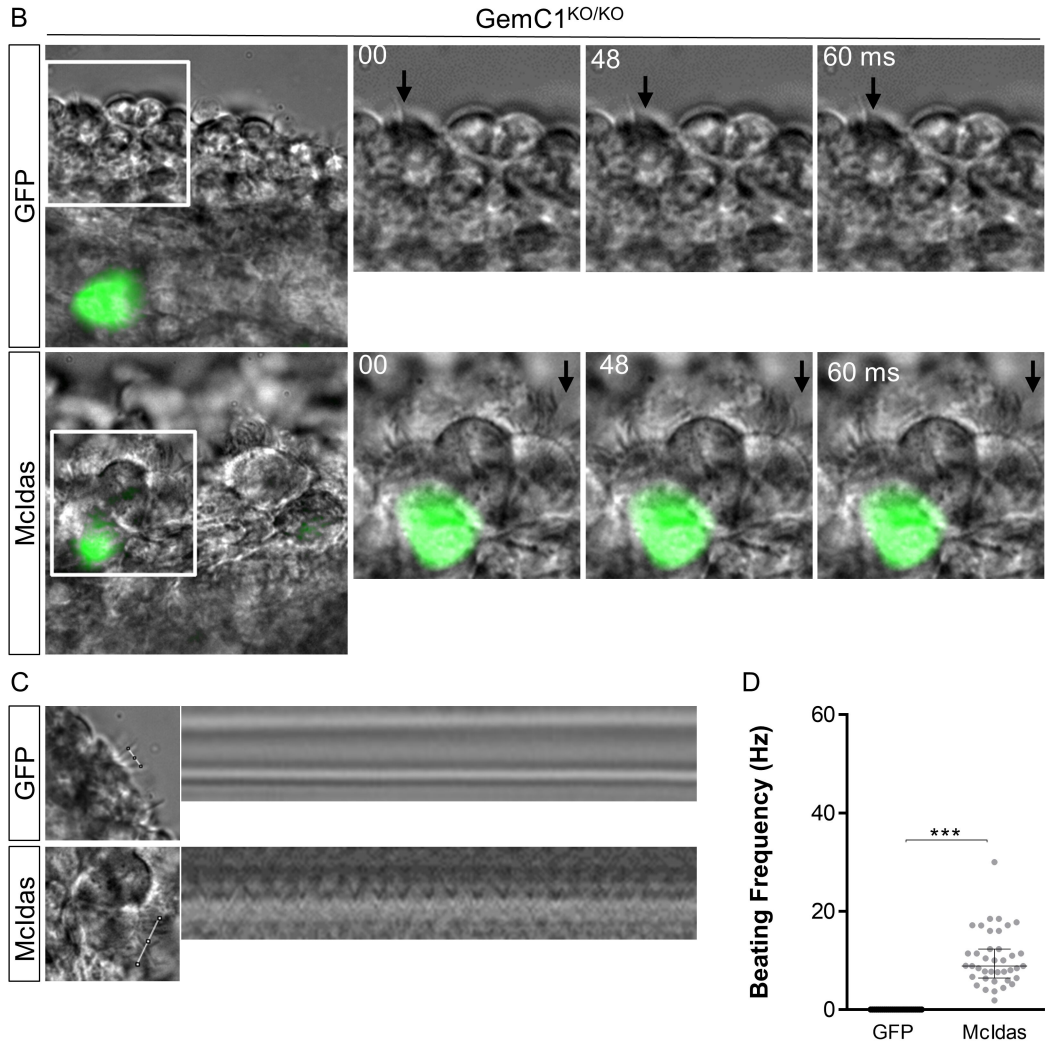
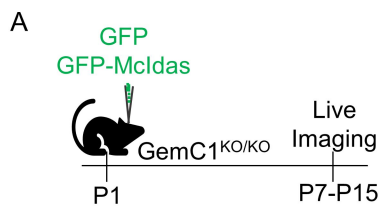
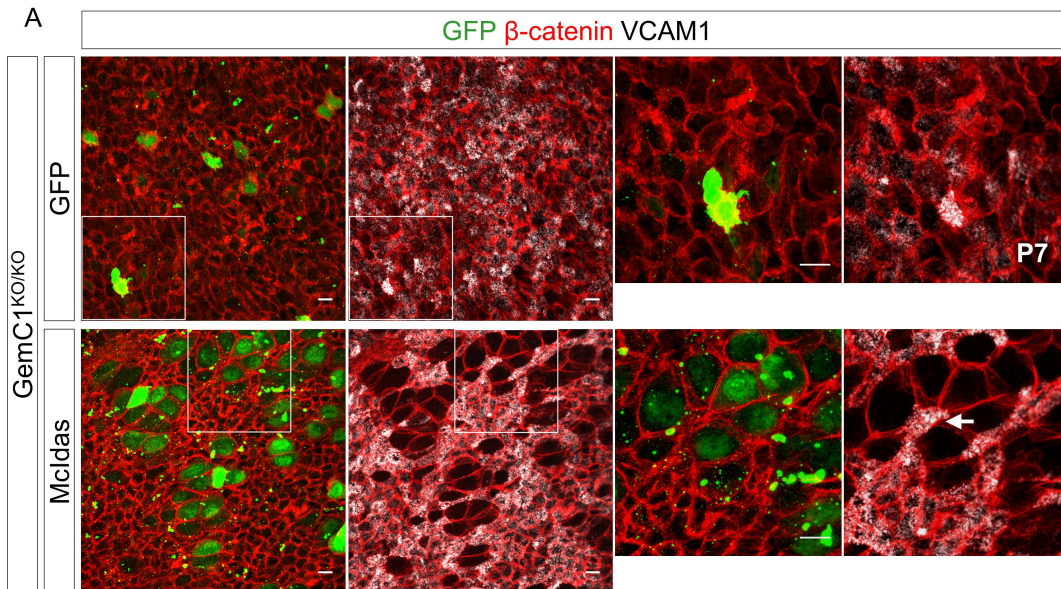
Figure 5

Figure 6

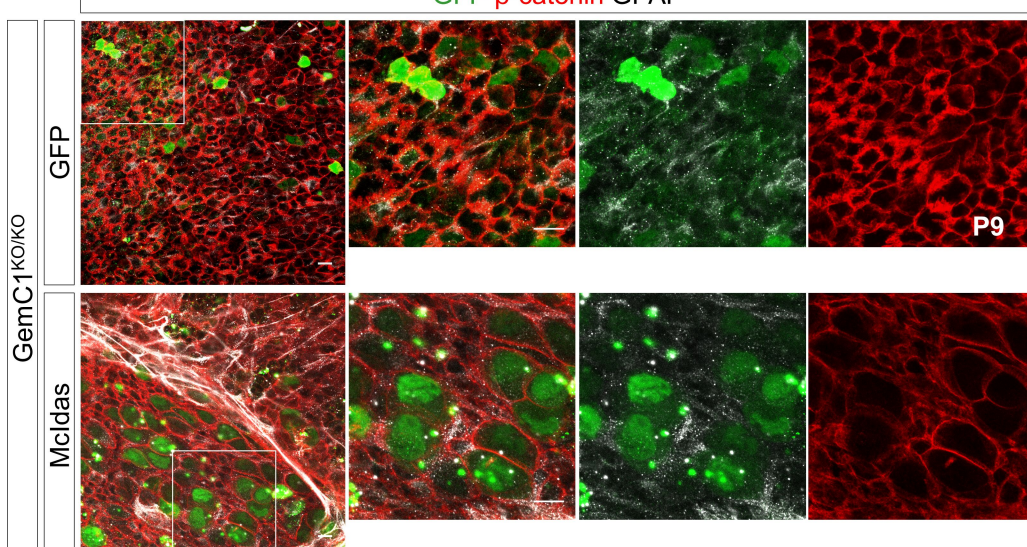
A

GFP β -catenin VCAM1



B

GFP β -catenin GFAP



C

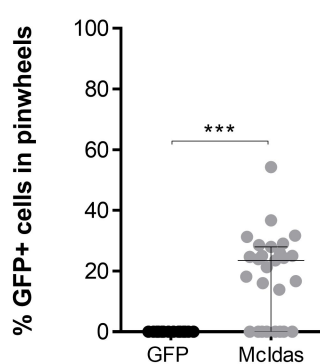


Figure EV1

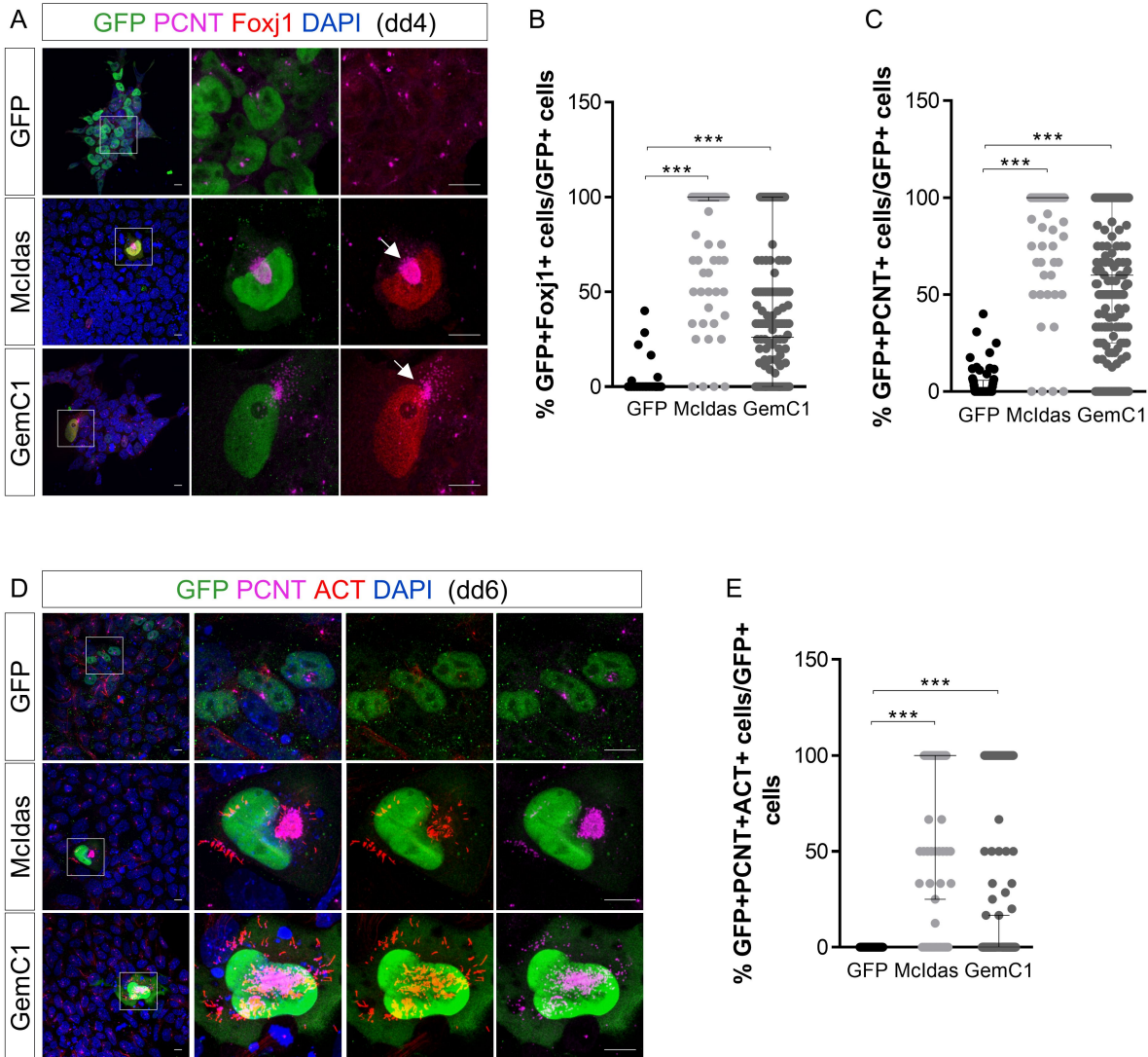


Figure EV2

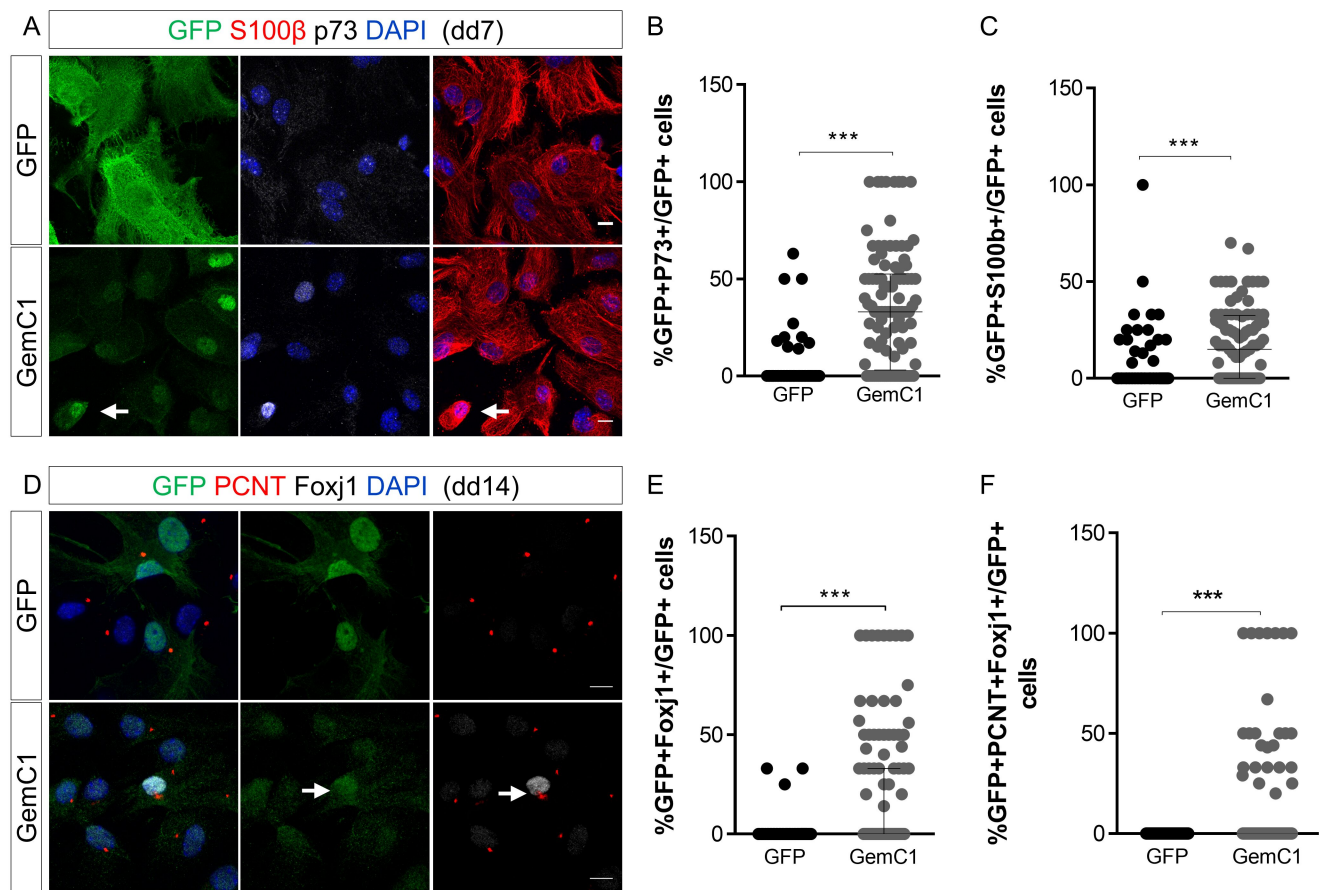


Figure EV3

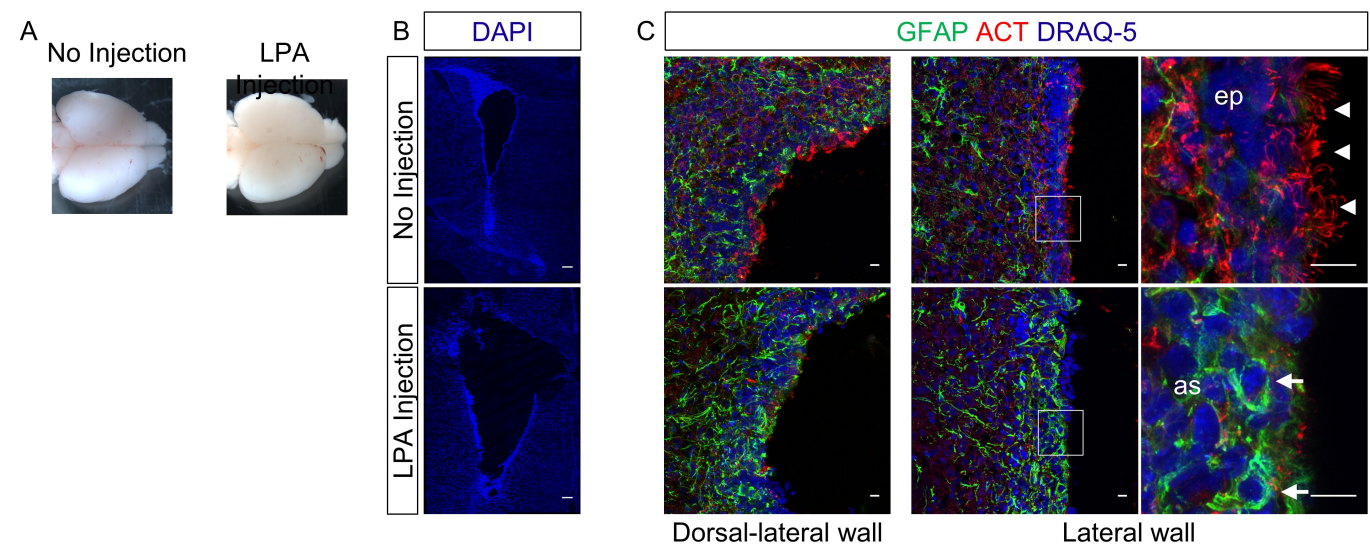


Figure EV4

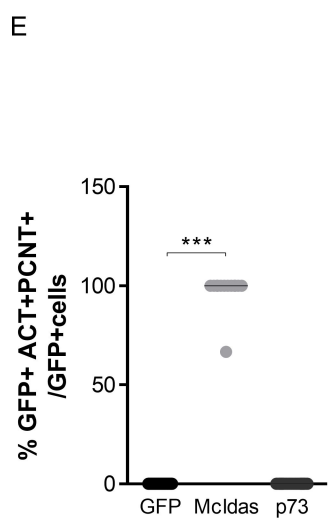
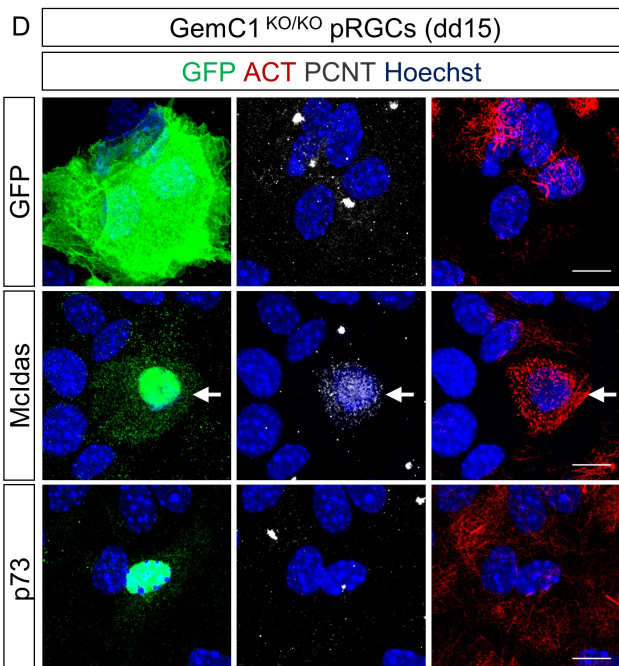
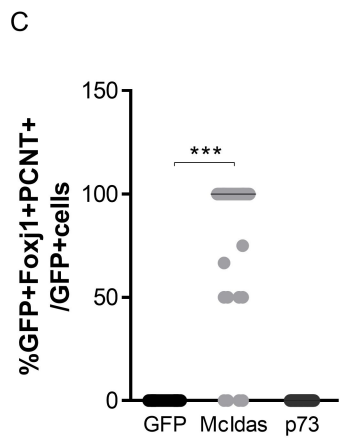
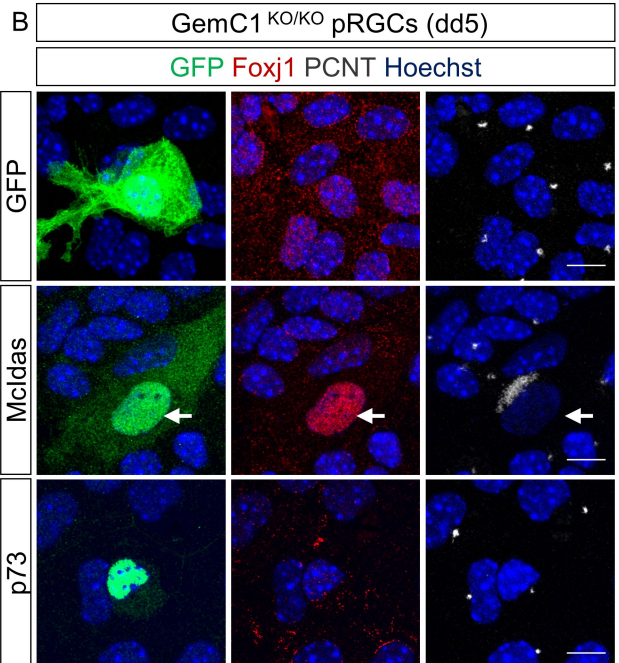
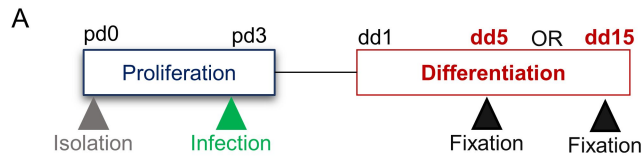


Figure EV5

